JAXA Research and Development Report

Calibration and Evaluation of Data from the Magnetometer (MGF) Onboard the Arase (ERG) Spacecraft

Ayako MATSUOKA and Masahito NOSÉ

March 2019

Japan Aerospace Exploration Agency

Contents

Preface

Preface

Ayako MATSUOKA[*1], Masahito NOSÉ[*2]

Precise magnetic field measurement is essential to investigate the space plasma phenomena. The same is true in the Arase (also known as Energization and Radiation in Geospace, ERG) project (Miyoshi et al., 2018) aiming to investigate the physical process of the relativistic electrons in the radiation belts. Magnetic Field Experiment (MGF, Figure 1) is required to precisely determine the magnetic field in the radiation belt; the field intensity error should be lower than 5 nT, and field direction error lower than 1° when we focus on the static magnetic field (Matsuoka et al., 2018). The MGF instrument as well as the spacecraft system were designed and manufactured to meet those requirements.
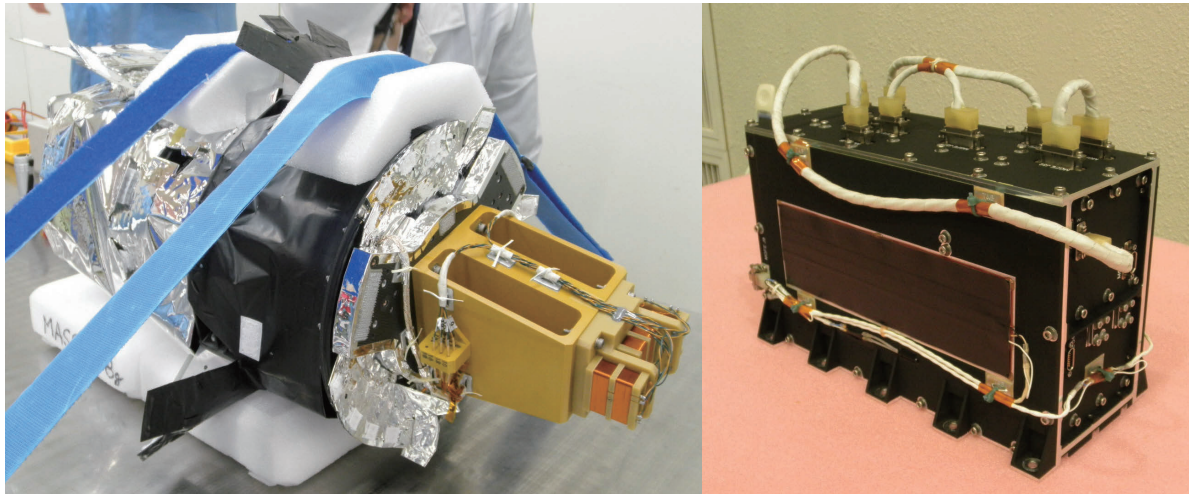

Fig. 1   (left) MGF sensor mounted on the extendable MAST   (right) MGF electronics box

While some of the MGF instrument characteristics are presented in Matsuoka et al. (2018), in this volume we describe the details about the instrument calibration, data evaluation and comparison with the geomagnetic models.

Sensitivity and alignment are basic parameters to be calibrated. Teramoto et al. (2019) and Matsuoka et al. (2019a) present the calibration results of the stand-alone MGF instrument. Teramoto et al. (2019) examined the sensitivity and inter-axis alignment in the room temperature. The sensitivity is determined within 0.07% accuracy and the alignment is within 0.03°. They examined the dependence of the relative sensitivity and offset on the sensor temperature as well. They show that the relative sensitivity is determined within 0.023% and the offset is within 0.67nT when we limit the temperature range between −10° and 0° which is very common as the MGF in-orbit environment. Matsuoka et al. (2019a) show the experimental results of the non-linearity characteristics of the analog-digital converter used for MGF. They examined the relation between the input analog signal and output digital value. The deviation from the linear relation is determined within 1.5 nT and 11.5 nT for ±8000 nT and ±60000 nT measurement ranges, respectively, when the environmental interference was not dominant.

To determine the accurate magnetic field direction in the absolute coordinate, we need to precisely convert the magnetic field measured by sensor elements into the absolute coordinate. Since the Arase spacecraft is spinning, the alignment of the measurement directions of MGF in the spacecraft coordinate may be computed from the in-orbit MGF data. Matsuoka et al. (2019b) determined the alignment angles with the accuracies better than 0.05° and 0.2° for ±8000 nT and ±60000 nT measurement ranges, respectively. They derive the conversion matrix based on the analysis results. Matsuoka et al. (2019c) provides the each procedure to compute the alignment angles.

The Arase spacecraft was developed with consideration of the magnetic cleanliness. The DC component of spacecraft-origin magnetic field noise at the MGF instrument has been measured at 2.5-m distance from the center of the powered-off spacecraft in the magnetic shielding chamber at JAXA's Sagamihara Campus (Matsuoka et al., 2018). It was estimated that the field intensity at the MGF position after 5-m MAST

deployment will be 0.18 nT. Nevertheless, it is also of great interest to examine the spacecraft-origin magnetic field noise during the operation. Yamamoto et al. (2019) and Oimatsu et al. (2019) performed comparison between the MGF observations and the magnetic model fields (Tsyganenko 89 and Tsyganenko-Sitnov 04) to estimate the magnetic field noise. Assuming that the MGF data are calibrated in terms of the sensor offset, the sensor sensitivity, and the sensor alignment, Yamamoto et al. (2019) and Oimatsu et al. (2019) found that the difference between the observations and models (observations minus models) is approximately −0.3 nT to 0.7 nT on average. These differences are caused by the spacecraft-origin magnetic field noise and/or the inaccuracy of the models. Therefore, they conclude that the spacecraft-origin magnetic field noise is quite small (a few tenths of nT) and consistent with the estimation by Matsuoka et al. (2018).

This volume coherently provides the information about the quality of the static magnetic field data obtained by Arase MGF. It would be worth referring for people who use the MGF data for scientific studies and other purposes.

REFERENCES

Ayako Matsuoka, Mariko Teramoto, Reiko Nomura, Masahito Nosé, Akiko Fujimoto, Yoshimasa Tanaka, Manabu Shinohara, Tsutomu Nagatsuma, Kazuo Shiokawa, Yuki Obana, Yoshizumi Miyoshi, Makoto Mita, Takeshi Takashima and Iku Shinohara, The ARASE (ERG) magnetic field investigation, Earth, Planets and Space, 70:43, 10.1186/s40623-018-0800-1, 2018.

Ayako Matsuoka, Mariko Teramoto and Reiko Nomura, Non-linearity Characteristics of the Analog-to-Digital Converter for Arase (ERG) Magnetometer (MGF), JAXA Research and Development Report, JAXA-RR-18-005E, 10.20637/JAXA-RR-18-005E/0002, 2019a.

Ayako Matsuoka, Mariko Teramoto and Reiko Nomura, In-orbit Alignment Analysis of the Magnetometer Sensor on the Arase (ERG) Satellite, JAXA Research and Development Report, JAXA-RR-18-005E, 10.20637/JAXA-RR-18-005E/0003, 2019b.

Ayako Matsuoka, Mariko Teramoto and Reiko Nomura, Method to Determine the In-orbit Sensor Alignment of the Magnetometer Onboard a Spin-stabilized Satellite (Japanese), JAXA Research and Development Memorandum, JAXA-RM-18-008, 10.20637/JAXA-RM-18-008/0001, 2019c.

Miyoshi, Y., I. Shinohara,, T. Takashima, K. Asamura, N. Higashio, T. Mitani, S. Kasahara, S. Yokota, Y. Kazama, S.-Y. Wang, S. W. Tam, P. T. P Ho, Y. Kasahara, Y. Kasaba, S. Yagitani, A. Matsuoka, H. Kojima, H. Katoh, K. Shiokawa, and K. Seki, Geospace Exploration Project ERG, Earth Planets Space, 2018.

Satoshi Oimatsu, Kazuhiro Yamamoto, Masahito Nosé, Ayako Matsuoka, Mariko Teramoto, and Shun Imajo, DC component of spacecraft-origin magnetic field noise at the Arase/MGF sensor: (2) Evaluation with Tsyganenko-Sitnov 04 model, JAXA Research and Development Report, JAXA-RR-18-005E, 10.20637/JAXA-RR-18-005E/0005, 2019.

Mariko Teramoto, Ayako Matsuoka and Reiko Nomura, Re-evaluation of the ground calibration for the Arase Magnetic Field Experiment, JAXA Research and Development Report, JAXA-RR-18-005E, 10.20637/JAXA-RR-18-005E/0001, 2019.

Kazuhiro YAMAMOTO, Satoshi OIMATSU, Masahito NOSÉ, Ayako MATSUOKA, Mariko TERAMOTO, and Shun IMAJO, DC component of spacecraft-origin magnetic field noise at the Arase/MGF sensor: (1) Evaluation with Tsyganenko 89 model, JAXA Research and Development Report, JAXA-RR-18-005E, 10.20637/JAXA-RR-18-005E/0004, 2019.

Re-evaluation of the ground calibration for
the Arase magnetic field experiment

Mariko TERAMOTO[*1], Ayako MATSUOKA[*2], Reiko NOMURA[*3]

ABSTRACT

Herein, ground calibration experiments were performed to determine the sensitivity for all components and the angles (alignment) between the measurement axes of the magnetic field experiment (MGF) onboard Arase satellite. We can well determine the sensitivities within 0.07 % error and the alignment within $90 \pm 1°$ with ~0.03° accuracy. Also, the temperature dependences of the offset and sensitivity were examined. Results revealed that the relative sensitivity to the room temperature can be fit with a linear regression line. The offsets exhibited systematical dependences on temperatures. Between March 13, 2017 and April 30, 2018, when MGF with an 8000-nT range mostly measured ambient magnetic field in orbit at -10°C–0°C, the linearity of sensitivity and offset with a standard error of < 0.00023 and <0.67 nT, respectively, was determined. The measured sensitivity, alignment, and offset were used to measure the magnetic field with high accuracy, thereby meeting the MGF capability and performance requirement of the field intensity <5 nT and the field direction error <1°.

1. Introduction

The Arase (ERG) satellite, developed by the Institute of Space and Astronautical Science (ISAS)/Japan Aerospace Exploration Agency (JAXA), was successfully launched on December 20, 2016 (Miyoshi et al., 2018) [1]. The magnetic field experiment (MGF) (Matsuoka et al., 2018)[2] onboard the Arase was performed to record the ambient magnetic field in the region since March 2017. Table 1 lists the design specifications of the MGF that comprises a sensor (MGF-S) and an electronic box (MGF-E). To investigate the particle acceleration processes in the inner magnetosphere, Arase must measure magnetic field with the magnetic field intensity error of <5 nT and an error in its direction of <1° when the satellite is located at L > 2.

The sensitivity of the MGF can be roughly estimated using the winding number of the pickup coil of the MGF-S and resistance of the feedback resistor of MGF-E. However, the exact sensitivities for the MGF should be determined on the ground by examining its response to a calibrated magnetic field. In addition, the axes of MGF-S are not orthogonal because three sensor elements were mounted on the sensor base with slight angle mismatch. To observe the magnetic field data in the orthogonal coordinate system, the alignment of each fluxgate sensor axis in a ground experiment must be examined. The temperature dependence of sensitivity and offset of the MGF must also be evaluated because the fluxgate system has a large temperature dependency.

Before Arase was launched, Teramoto et al. (2017)[3] determined the sensitivity and alignment of MGF-S on Arase along with the temperature dependence of the sensitivity and offset. The errors were evaluated via ground calibration experiments. MGF/Arase can obtain the actual magnetic field data for the inner magnetosphere in more than one year. Herein, the methods and results of the ground calibration experiments are summarized and the error values for the actual MGF observations are re-evaluated.

Table 1 MGF design specifications

sensor	ring-core
dynamic range	range-0: ±8000 nT
	range-1: ±60000 nT
resolution	range-0: 114 pT
(20 bit)	range-1: 15 pT
noise level	<10.5 pT/Hz$^{-0.5}$@1Hz
sampling rate	256 Hz

2. Ground calibration of MGF for sensor alignment and sensitivity determination

2.1. Methods

The principle and method for the ground calibration of the three-axis fluxgate magnetometer were first proposed by Acuna et al(1978)[4]. Following the method proposed by Yamamoto et al (1996)[5], we examined the output relative to the known magnetic field applied by the calibration coil. We determined the sensitivity and alignment of the magnetometer and also the direction of the calibrated magnetic field, using two orthogonal calibration mirrors.

The relationship between the relating parameters, namely the sensitivity of MGF-S [A_i(i=x,y,z)] (nT/digit), output of MGF-S [M_i] (digit), the transform matrix from the alignment mirror coordinate attached MGF-S to the sensor coordinate $\vec{\varepsilon}$, the transform matrix from the alignment mirror coordinate of the coil to the alignment mirror coordinate of the sensor [$\mathbf{K}$], the transform matrix from the calibration coil to the calibration mirror attached calibration coil $\vec{\delta}$, the applied magnetic field [B_i] (nT), and the zero-offsets [$B_{o,i}$] (nT), is described as follows:

$$
\begin{pmatrix} A_x & 0 & 0 \\ 0 & A_y & 0 \\ 0 & 0 & A_z \end{pmatrix} \begin{pmatrix} M_x \\ M_y \\ M_z \end{pmatrix} = \vec{\varepsilon} \cdot \mathbf{K} \cdot \vec{\delta} \begin{pmatrix} B_x \\ B_y \\ B_z \end{pmatrix} + \begin{pmatrix} B_{o,x} \\ B_{o,y} \\ B_{o,z} \end{pmatrix}
\tag{1}
$$

Equation (1) describes the applied magnetic field [B_i] and the relationship between the alignment mirror coordinates of the coil and the sensor, $\mathbf{K}$. The output of MGF-S is known. The zero-offset of MGF-S, [$B_{o,i}$], is ignored because of the linearity between the inputs and the outputs of the applied magnetic field intensities. Thus, a total of 21 unknown parameters among [A_i], $\vec{\varepsilon}$, and $\vec{\delta}$ need to be determined.

Using the angles of the directions of the MGF-S and the calibration coil to those of calibration mirrors, as shown in Figure 1, $\vec{\varepsilon}$ and $\vec{\delta}$ are written as

$$
\vec{\varepsilon} = \begin{pmatrix} 1+\varepsilon_{xx} & \varepsilon_{xy} & \varepsilon_{xz} \\ \varepsilon_{yx} & 1+\varepsilon_{yy} & \varepsilon_{yz} \\ \varepsilon_{zx} & \varepsilon_{zy} & 1+\varepsilon_{zz} \end{pmatrix} = \begin{pmatrix} \cos\theta_x \cos\phi_x & \cos\theta_x \sin\phi_x & \sin\theta_x \\ \cos\theta_y \sin\phi_y & \cos\theta_y \cos\phi_y & \sin\theta_y \\ \cos\theta_z \sin\phi_z & \sin\theta_z & \cos\theta_z \cos\phi_z \end{pmatrix}
\tag{2}
$$

and

$$
\vec{\delta} = \begin{pmatrix} 1+\delta_{xx} & \delta_{xy} & \delta_{xz} \\ \delta_{yx} & 1+\delta_{yy} & \delta_{yz} \\ \delta_{zx} & \delta_{zy} & 1+\delta_{zz} \end{pmatrix} = \begin{pmatrix} \cos\lambda_x \cos\varphi_x & \cos\lambda_y \sin\varphi_y & \cos\lambda_z \sin\varphi_z \\ \cos\lambda_x \sin\varphi_x & \cos\lambda_y \cos\varphi_y & \sin\lambda_z \\ \sin\lambda_x & \sin\lambda_y & \cos\lambda_z \cos\varphi_z \end{pmatrix}
\tag{3}
$$

$\vec{\varepsilon}$ and $\vec{\delta}$ are very close to unit matrices. Six conditions are described in (2) and (3) because the row and column vectors in $\vec{\varepsilon}$ and $\vec{\delta}$ are unit vectors, respectively.

From one experimental setup, i.e. one **K** and **B** in the x, y, and z directions, independently, nine equations can be obtained from equation (1). From the conditions obtained from (2) and (3), 15 equations in total are obtain. If the MGF-S is rotated 90° with respect to one of the coordinates, nine more equations can be obtained. However, only six equations among these nine equations are independent of the previous (un-rotated) setup. Consequently, 21 conditions are obtained in total for the 21 parameters. Although the number of conditions is sufficient to determine 21 unknown parameters, one more experimental setup (rotations of MGF-S around another axis) is required to solve the equations more reliably and stably. The alignment and sensitivity parameters are determined using the 27 conditions obtained via three-setup experiments.
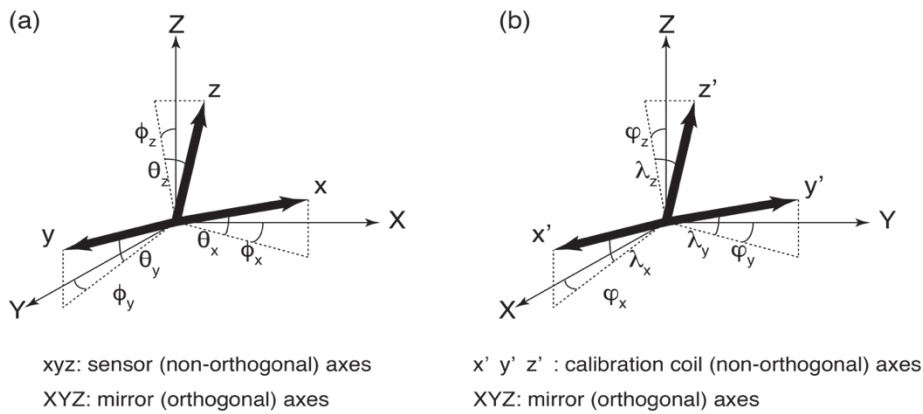

xyz: sensor (non-orthogonal) axes
XYZ: mirror (orthogonal) axes

x' y' z' : calibration coil (non-orthogonal) axes
XYZ: mirror (orthogonal) axes

Fig. 1. Definitions of the angle (a) MGF-S and sensor mirror coordinates (b) calibration coil and coil mirror coordinates

2.2. Settings

The MGF was calibrated in the three-axis, 15-m Braunbeck coil system of the magnetic test facility at Tsukuba Space Center, JAXA, from March 2 to March 5, 2016. The Braunbeck coil system can create an almost-zero magnetic field environment in the center of this coil system by canceling the geomagnetic field and its disturbances. A three-axis Helmholtz coil system (calibration coil), which can produce the magnetic field within an accuracy of 0.1% in each direction, is installed at the center of the Braunbeck coil system to apply the magnetic field for calibration. The MGF-S on a rotation table was set at the center of the calibration coil. The cubic calibration mirrors were attached onto the calibration coil and turn table in order to setup the experiments with high accuracy using the laser alignment system.

When the **K** coordinate system of MGF-S (Figure 2) was set by rotating the table, the mirror coordinates were adjusted to match their alignment with high accuracy using the lazier alignment system installed 16 m away from the center of the calibration coil. After the mirror adjustment, the output of MGF-S was measured relative to the applied magnetic field (Table 2). The experiments were performed thrice for the ±8000-nT range and twice for ±60000-nT range at the room temperature (21.4°C).

Table 2. Applied fields during the calibration experiment

Range	Applied field (nT)
±8000-nT range	0, ±7000, ±5200, ±2600
±60000-nT range	0, ±50000 ±3000

$$K^1 = \begin{pmatrix} 0 & 0 & -1 \\ 0 & -1 & 0 \\ 1 & 0 & 0 \end{pmatrix} \quad K^2 = \begin{pmatrix} 0 & 0 & -1 \\ -1 & 0 & 0 \\ 0 & 1 & 0 \end{pmatrix} \quad K^3 = \begin{pmatrix} -1 & 0 & 0 \\ 0 & 1 & 0 \\ 0 & 0 & 1 \end{pmatrix}$$
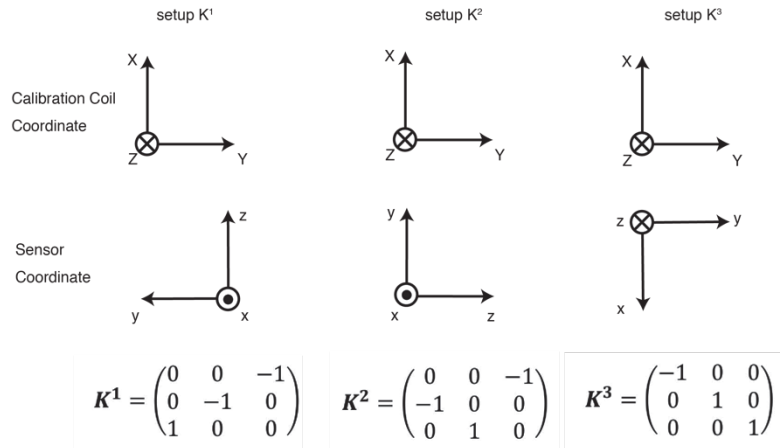
Fig. 2. Configurations of the coil and the sensor

2.3. Results

Figure 3 shows an example of the MGF output (M_i) relative to the applied magnetic field (B_i) (K1, K2, or K3) for one experiment. Mi is the 10-s averaged data. As expected in equation (1), we find clear linearities between the input and output magnetic fields. We confirmed that such linearity holds for all experiments with ±8000-nT and ±60000-nT ranges. The output matrix **M** in the equation (1) is obtained from the inclination of the M relative to B. The standard errors between regression lines and the measurements are within 0.05% for all experiments.
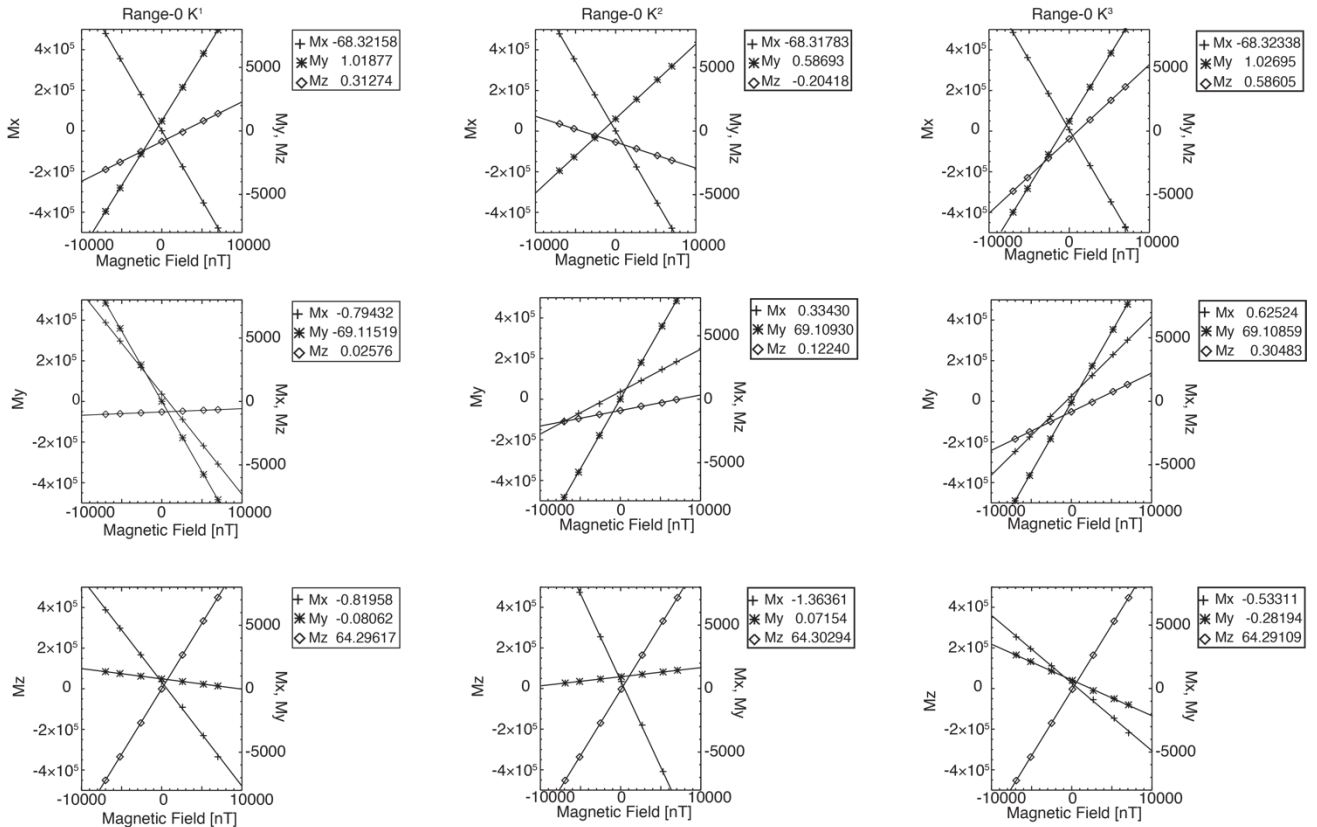

Fig.3 Output M relative to the applied magnetic field B within 8000-nT range

2.3.1. Sensitivity

Table 3 shows the sensitivities and the relative errors in the 60000-nT and 8000-nT ranges obtained from

the equations (1), (2), and (3). The sensitivities of both ranges were well determined with an error of < 0.07 %. The maximum error of 0.06 % with the 8000-nT range indicates that the analytical errors are <4.8 nT when MGF is used to observe magnetic field at the intensity of 8000 nT, which is within the required error of 5 nT for Arase.

Using the actual magnetic field data measured in the magnetosphere by MGF with the ±8000-nT range from March 13, 2017 to April 30, 2018, we investigated the magnetic field intensity measured by Arase. We found that the magnetic field intensities measured by MGF (with the 8000 nT range) are at less than 1000 nT in most cases: at 91.0%, 91.3 %, and 90.3% of the total measurement time for X, Y, and Z components respectively. This result indicates that the analytical error of MGF due to determination of sensitivity is less than 0.6 nT. We conclude that most of the 8000nT range measurements meet the observational requirement for Arase.

<div align="center">Table 3. Sensitivity of MGF-S/Arase</div>

	X component		Y component		Z component	
	Sensitivity (nT/digit)	Error (%)	Sensitivity (nT/digit)	Error (%)	Sensitivity (nT/digit)	Error (%)
60000-nT range	0.1072	0.03	0.1057	0.07	0.1137	0.04
8000-nT range	0.01464	0.06	0.01447	0.06	0.01555	0.05

2.3.2. Alignment of the MGF-S

The determined angles between the MGF-S and calibration mirror alignments with each range are summarized in Tables 4. While ϕ_x, ϕ_y, ϕ_z, and θ_z of the 8000-nT range are almost similar to those of the 60000-nT range, θ_x and θ_y for the 8000-nT range are respectively 0.57° and 0.08° smaller than those of the 60000-nT range. Due to the differences in these angles, Y-Z and Z-X angles of the 8000-nT range are 0.1° and 0.54° larger than those of the 60000-nT range, respectively, as shown in Table 5. Thus, a different alignment must be applied for each range when we calibrate the in-flight data of MGF in orbit. As shown in Table 4, we can determine the alignment with a high accuracy, i.e., the estimated error is <0.03° for both ranges.

In addition to the analytical error of the abovementioned alignments, we need to evaluate the alignment error from the experimental equipment. The coordinate system of MGF-S has an alignment error within 0.03° relative to the calibration coil because the plane of turn table, onto which MGF-S and the calibration mirror were attached, has a slight difference from the horizontal. Further, the adjustment of the coordination system using the laser system has the alignment error within the 0.03°. Thus, the alignment error from the experiment equipment is <0.07°. Even though the additional error from the experimental equipment is included in the total alignment error, we determined the alignment error to be <0.1°, which is sufficient to meet the observational requirements.

<div align="center">Table 4. Obtained angles for sensor-mirror alignment. Unit is degrees</div>

	θ_x	ϕ_x	θ_y	ϕ_y	θ_z	ϕ_z
60000-nT range	-0.15 ± 0.03	0.23 ± 0.003	0.26 ± 0.004	-0.43 ± 0.01	-0.12 ± 0.02	-0.26 ± 0.01
8000-nT range	-0.72 ± 0.02	0.25 ± 0.03	0.18 ± 0.004	-0.44 ± 0.006	-0.15 ± 0.006	-0.23 ± 0.03

<div align="center">Table 5. Angle between the axes. Unit is degrees</div>

	∠XY	∠YZ	∠ZX
60000nT range	90.20	89.86	90.41
8000nT range	90.19	89.97	90.95

2.3.3. Alignment of the calibration coil

The obtained angles between the calibration coil and calibration mirror alignments and the relative angles between axes of calibration coil are summarized in Tables 6 and 7, respectively. The obtained and relative

angles do not show significant differences between different ranges. The relative angles are within 0.01°, indicating that the relative angles of the calibration coil are estimated with high accuracy.

Table 6. Obtained angles for coil-mirror angle. Unit is degrees.

	ψ_x	λ_x	ψ_y	λ_y	ψ_z	λ_z
60000-nT range	-0.04 ± 0.02	0.44 ± 0.001	0.42 ± 0.02	-0.29 ± 0.06	-0.42 ± 0.001	0.06 ± 0.05
8000-nT range	-0.04 ± 0.007	0.42 ± 0.002	0.42 ± 0.006	-0.28 ± 0.02	-0.41 ± 0.002	0.05 ± 0.04

Table 7. Angle between axes of calibration coil. Unit is degrees.

	$\angle XY$	$\angle YZ$	$\angle ZX$
60000-nT range	89.86	89.99	89.98
8000-nT range	89.86	89.99	89.99

3.   Temperature dependence of the sensitivity and offset

3.1. Methods

We can derive the temperature dependence of the sensor by measuring the output of the MGF, $\mathbf{M}_{app}$, before and after applying external magnetic field, $\mathbf{B}_{app}$, with a Helmholtz coil in a space, which is left approximately zero ($\mathbf{B}_{env}$). Given that the output, offset, and sensitivity at room temperature (and at a temperature t) are $\mathbf{M}_{app,o}$ ($\mathbf{M}_{app,t}$), and $\mathbf{M}_{0,o}$ ($\mathbf{M}_{0,t}$), and $\mathbf{a}_o$ ($\mathbf{a}_t$) respectively, $\mathbf{M}_{app,o} = \mathbf{a}_o(\mathbf{B}_{app}+\mathbf{B}_{env}) + \mathbf{M}_{0,o}$ and $\mathbf{M}_{app,t} = \mathbf{a}_t(\mathbf{B}_{app}+\mathbf{B}_{env}) + \mathbf{M}_{0,t}$. Therefore, the relative sensitivity of a temperature (t) to room temperature is given as

$$\frac{\mathbf{a}_t}{\mathbf{a}_o} = \frac{\mathbf{M}_{app,t} - \mathbf{M}_{0,t}}{\mathbf{M}_{app,o} - \mathbf{M}_{0,o}} \tag{4}.$$

The offset of the MGF-S is obtained by the output in both the normal and the reverse directions in the stably almost-zero magnetic field ($\mathbf{B}_{env}$). Given that the MGF-S outputs in the normal and reverse directions at the temperature of t are

$$\mathbf{M}_{n,t} = \mathbf{a}_t\mathbf{B}_{env} + \mathbf{M}_{0,t} \tag{5}$$

$$\mathbf{M}_{r,t} = -\mathbf{a}_t\mathbf{B}_{env} + \mathbf{M}_{0,t} \tag{6},$$

the offset at a certain temperature is obtained by

$$\mathbf{M}_{0,t} = \frac{\mathbf{M}_{n,t} + \mathbf{M}_{r,t}}{2} \tag{7}$$

We can estimate temperature dependence of relative sensitivity and offset of the MGF-S, by measuring $\mathbf{M}_{n,t}$, $\mathbf{M}_{r,t}$, and $\mathbf{M}_{app,t}$ at various temperature around the MGF-S.

3.2. Setting

The temperature experiment was performed from February 8 to February 12, 2016 in a magnetic shielding chamber at ISAS, JAXA. The magnetic field in this chamber made of triple-layer permalloy is stably <30 nT. We used the similar equipment and method as the temperature experiments for MMO/MGF[6]. The three coils of MGF-S detached from the pedestal were installed in parallel to each other on a ceramic disk. The two thermopiles for monitoring temperature around the MGF-S was attached to the disk across the MGF-S. We controlled temperature in the thermos bottle with a ceramic lid, in which the disk was confined. This thermos bottle was placed between the applied coils which induced the magnetic field around the MGF-S with a 20-mA current. The thermos bottle and the applied coils were placed a turn table, by which MGF-S can be rotated and reversed.

In higher-temperature measurements, we heated the thermos bottle to 45°C using a heat gun. After keeping the thermos bottle at 45°C for 30 min, the heat gun was removed from the thermos bottle; then, the experiment was performed as the ambient temperature in the bottle decreased by 5°C. In the low-temperature measurements, the bottle was cooled using dry ice. After stuffing 90-g crushed dry ice uniformly between the bottle and the disk, measurements were performed (at every 5°C interval) when the temperature in the bottle began increasing.

When the temperature in the bottle increases or decreases by 5°C, we measured the temperature and the output of MGF-S for the following three situations :(a) at the normal position with no applied magnetic field; (b) at the normal position with an applied magnetic field; and (c) at the reverse position with no applied magnetic field, as illustrated in Figure 4. In situation (a), each component of MGF-S measured an ambient magnetic field of <30 nT in the magnetic shield chamber. These outputs correspond to $M_{n,t}$. In situation (b), MGF-S observed the total magnetic field of the ambient magnetic field in the chamber and the applied magnetic field generated by the calibration coil. This output is $M_{app,t}$. Rotating the turn table horizontally by 180°, we set the MGF-S for the situation (c). The MGF-S observed the ambient magnetic field of the magnetic shielding room in the opposite direction to one in the situation (a). This output corresponds to $M_{r,t}$.
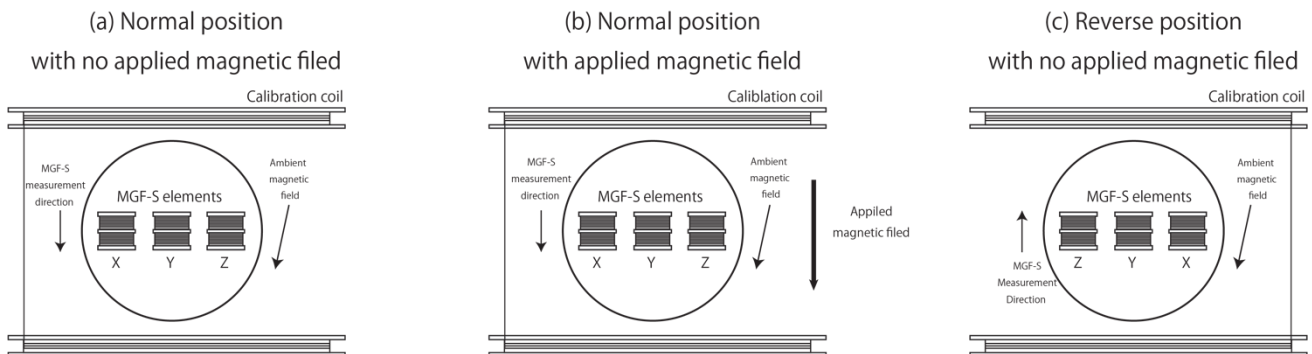

Fig 4. Each position of the MGF-S in the temperature experiments

3.3. Results

We performed temperature experiments thrice (Experiments 1, 2, and 3) within -20°C–30°C, which is expected temperature range for the MGF observation in the inner magnetosphere. We used the 8-s average outputs of the MGF with the-8000 nT range.

3.3.1. Relative sensitivities

Figure 5 represents the temperature dependences of the relative sensitivities in X, Y, and Z components of MGF-S. We only showed the measurements from Experiment 1, in which the dispersions of the measurements from the liner regression model is the smallest among all the experiments. We determined the following linear expressions from the measurements in Experiment 1 as

$$r_x = 4.8577 \times 10^{-5}t + 0.99876$$
$$r_y = 4.9017 \times 10^{-5}t + 0.99878 \tag{8}$$
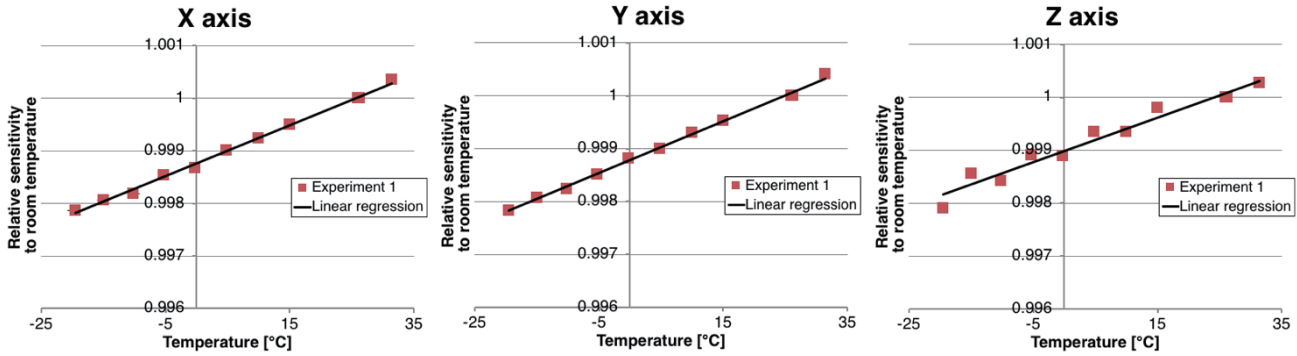$$r_z = 4.2169 \times 10^{-5}t + 0.99998$$

Fig. 5. Temperature dependence of sensitivity. Ratio to the sensitivity to the room temperature 26.1 °C is shown
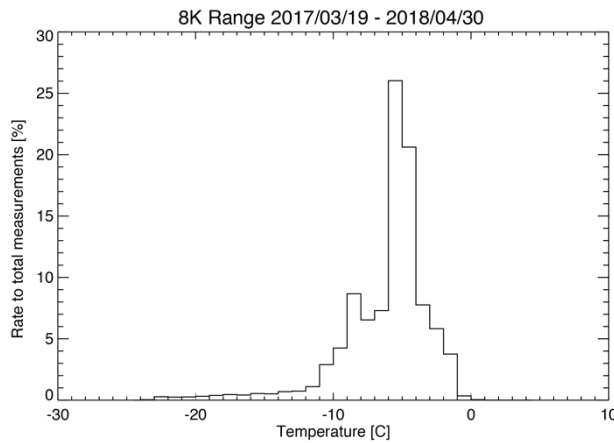

Fig. 6. Histogram of the rate of total measurements of MGF 8000-nT range between March 19, 2017 and April 30, 2018

Then, we considered the errors of the sensitivity applying temperature dependence as expressed as (8). Tables 8 and 9 represent the standard errors from the regression lines and the measurement errors of the MGF for the observations of the 8000-nT ambient magnetic field. The standard error of the Z component of the MGF (1.3 nT in the 8000-nT magnetic field intensity) is the largest among all the components between -20°C and 30°C.

In the in-flight measurements, the temperatures of the MGF-S are expected to be mostly higher than -10°C, except for the case with the long-term shading. Figure 6 represents the histogram of the MGF-S temperature with a bin width of 1°C when the MGF measured magnetic field in flight with 8000-nT range from March 19, 2017 to April 30, 2018. As expected, 91.1%, of MGF data were obtained between -10°C and 0°C.

As shown in Tables 8 and 9, we evaluated the standard errors of the temperature dependence of the sensitivity in three categories: from -20°C to -10°C, from -10 to 0°C, and from 0°C to 30°C. The standard errors of the relative sensitivities in all components decrease as the temperature increases. Table 8 shows that the standard error from the regression lines is less than 0.00023 between -10°C and 0°C. As shown in Table 9, the uncertainty due to the temperature dependence within -10°C–0°C is <1.9 nT when the MGF observed the magnetic field intensity of 8000 nT. The uncertainty due to the temperature dependence sufficiently matches the requirements of Arase.

Table 8. Standard errors for temperature dependence.

	X	Y	Z
-20°C–30°C	$\pm7.9943 \times 10^{-5}$	$\pm5.8729 \times 10^{-5}$	$\pm1.6558 \times 10^{-4}$
-20°C–-10°C	$\pm1.7606 \times 10^{-4}$	$\pm6.1742 \times 10^{-5}$	$\pm3.8642 \times 10^{-4}$
-10°C–0°C	$\pm1.0387 \times 10^{-4}$	$\pm6.5215 \times 10^{-5}$	$\pm2.3393 \times 10^{-4}$
0°C–30°C	$\pm7.2412 \times 10^{-5}$	$\pm7.3208 \times 10^{-5}$	$\pm1.5327 \times 10^{-4}$

Table 9. Uncertainty due to the temperature dependence for 8000 nT.

	X	Y	Z
−20°C–30°C	±0.64	±0.47	±1.3
−20°C–−10°C	±1.4	±0.49	±3.1
−10°C–0°C	±0.83	±0.52	±1.9
0°C–30°C	±0.58	±0.59	±1.2

3.3.2. Offset

  Figure 7 shows the temperature dependence of the offset for each component, of which outputs are applied by sensitivity determined in Section 2.3.1 at 21.4°C and the temperature dependence as expressed as (8) and converted to physical value. While the offset seems to have some systematical dependences on temperature, it is difficult to find an ideal model to fit the experimental results with high accuracy. We determined the offset by averaging the experimental results, dividing temperature to three categories as mentioned in the previous sub-sections. The averaged offsets are 8.18, 10.5, and ˗10.6 nT for X, Y, and Z components, respectively, within ˗10°C–0°C, at which the MGF mostly obtains magnetic field data for the inner magnetosphere. The standard error analysis indicates that the determined offset of MGF-S has an uncertainty of <0.67 nT, which meets the requirement of MGF.
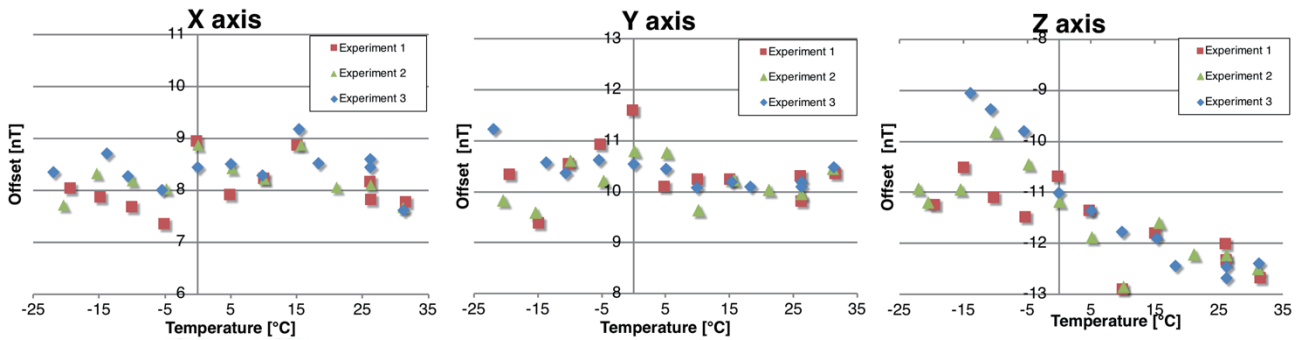

Fig. 7. Temperature dependence of the offset

Table 10. Averages and standard error of the offset in each directions of the MGF-S sensor.

	X		Y		Z	
	Averaged Offset	Standard Error	Averaged Offset	Standard Error	Averaged Offset	Standard Error
−20°C–30°C	8.23	±0.36	10.3	±0.44	−11.5	±0.56
−20°C–−10°C	8.04	±0.44	10.4	±0.67	−10.4	±0.97
−10°C–0°C	8.18	±0.54	10.5	±0.63	−10.6	±0.67
0°C–30°C	8.41	±0.36	10.2	±0.25	−12.0	±0.59

4. Summary and conclusion

Ground experiments were performed to obtain sensitivity and alignment data for the MGF onboard the Arase satellite and evaluated whether the determined sensitivity and alignment meet the scientific requirements for the Arase observation. The sensitivities for all component were determined in the 8000-nT and 60000-nT ranges with high accuracy using the method proposed by Yamamoto et al (1996)[5]. The analytical error of MGF sensitivity in the 8000-nT range is less <0.06%. Because MGF mostly operates in 8000-nT range at magnetic intensities of <1000nT, the magnetic intensities observed using MGF for each component have errors <0.6nT. The sensor axes are orthogonal to each other within 0.95° with an estimated error of <0.07°.

The temperature dependence of sensitivity and offset were also determined. Within -10°C–0°C, in which MGF mostly measured the magnetic field from March 13, 2017 to April 30, 2018, the sensitivities had a linearity to the temperature with a standard error of <0.00023. It indicates that in the 8000-nT range the MGF mostly observed the magnetic field with an uncertainty of <1.9 nT due to temperature dependence. The offset of the sensors has no clear linearity but reproducibility against temperature. The averaged offsets in the temperature from -10°C to 0°C are 8.18, 10.5, and -10.6 nT for the X, Y, and Z components, respectively. We can determine these offsets with a standard error of <0.67 nT.

These ground examinations show that the determination accuracies of the amplitude and direction of the magnetic field observed using the Arase/MGF satisfy the requirements for the Arase observations.

REFERENCE

[1] Miyoshi, Y., Shinohara, I., Takashima, T., Asamura, K., Higashio, N., Mitani, T., Kasahara, S., Yokota, S., Kazama, Y., Wang, S.-Y., Tam, S.W.Y., Ho, P.T.P., Kasahara, Y., Kasaba, Y., Yagitani, S., Matsuoka, A., Kojima, H., Katoh, Y., Shiokawa, K., and Seki, K., Geospace exploration project ERG, Earth, Planets and Space, 70:101 (2018).

[2] Matsuoka, A., Teramoto, M., Nomura, R., Nose, M., Fujimoto, A., Tanaka, Y., Shinohara, M., Nagatsuma, T., Shiokawa, K., Obana, Y., Miyoshi, Y., Mita, M., Takashima, T., and Shinohara, I., The ARASE(ERG) magnetic field investigation, Earth, Planets and Space, 70:43 (2018).

[3] Teramoto, M., Matsuoka, A., and Nomura, R., Ground calibration experiments of Magnetic field experiment on the ERG satellite, JAXA-RM-16-003 (2017).

[4] Acuna, M.H., MAGSAT–Vector Magnetometer Absolute Sensor Alignment Determination, NASA Goddard Space Flight Center X-754-83-9 (1978).

[5] Yamamoto, T., Kokubun, S., and GEOTAIL/PLANET-B MGF team, Ground Calibration of High-Sensitivity Magnetometers for Spacecraft Use, The Institute of Space and Astronautical Report, 88 (1996).

[6] Nishio, A., Usui, M., Tohyama, F., and Matsuoka, A., Wide-Temperature-Range Test of Fluxgate Magnetometer Sensor for Mercury Exploration, Proceeding of the School of Engineering of Tokai University, Vol. 46, No. 2 (2006), pp.123-128.

Non-linearity Characteristics of the Analog-to-Digital Converter for Arase (ERG) Magnetometer (MGF)

Ayako MATSUOKA[*1], Reiko NOMURA[*2], Mariko TERAMOTO[*3]

ABSTRACT

The high-resolution magnetic field measurement in the intense field is required for the achievement of the Arase project. The magnetometer (MGF) onboard Arase has the digital resolution of 20 bit, which is realized by the 20-bit analogue-to-digital conversion (ADC). A delta-sigma ADC circuit has been developed to satisfy the 20-bit resolution, 256 Hz sampling and tolerance for the severe radiation environment in the radiation belt. We performed the ground experiment at a room temperature to evaluate the non-linearity characteristics of the delta-sigma ADC used for MGF. The non-linearity error for the full range was measured by obtaining continuously the output digital values from ADC for gradually varying input analogue voltage. The maximum non-linear error was 781 digits (0.07% of the full range) corresponding to 11 nT (84 nT) for ±8000 nT (±60000 nT) measurement range. The deviation was determined within 103 digits, corresponding to 1.5 nT (11.0 nT) for ±8000 nT (±60000 nT) range, when the environmental interference noise was not intense. It is within 213 digits, corresponding to 3.1 nT (22.5 nT) for ±8000 nT (±60000 nT) range, when the environmental noise was significant.

1. ANALOG-TO-DIGITAL CONVERTER FOR ARASE MGF

The Arase (also known as Energization and Radiation in Geospace, ERG) satellite was launched primarily to reveal the generation and loss mechanisms of relativistic electrons in the earth radiation belts (Miyoshi et al., 2018a). The high-resolution magnetic field measurement in the intense field is required for the achievement of the Arase mission. The Magnetic Field Experiment (MGF) magnetometer for the Arase mission was developed to conduct precise measurements of the static magnetic field and low-frequency magnetic field variations. The details of the MGF instrument design and characteristics are presented in Matsuoka et al. (2018).

MGF has two dynamic ranges, ±8000 nT and ±60000 nT, and the digital resolution of 20 bits. It is realized by the 20-bit analogue-to-digital conversion (ADC). Although there are popular commercial ADC ICs of 20-bit resolution or higher, their tolerance in the high radiation environment has not been well proved. A delta-sigma ADC circuit composed by discrete parts has been developed to satisfy the 20-bit resolution, 256 Hz sampling and tolerance for the radiation environment in the radiation belt.

Figure 1 shows the block diagram of the delta-sigma ADC designed for MGF. It has almost same design as that for BepiColombo MMO MGF-I (Baumjohann et al., 2010) except the output sampling frequency. It consists of an analogue delta-sigma modulator and a Finite Impulse Response (FIR) filter. The delta-sigma modulation circuit is made from a 14-bit ADC and a 12-bit Digital-to-Analogue Converter (DAC). It generates raw data with 16 kHz as the output of 14-bit ADC. The modulated data are fed back to the DAC and subtracted from the next input data value. The FIR filter implemented in a field-programmable gate array (FPGA) processes the digitised data and outputs the 256 Hz digital data with 20 bit resolution.

The error of ADC causes the error of the magnetic field measured by MGF. We carried a ground experiment of the MGF flight model to evaluate the non-linearity characteristics of ADC.
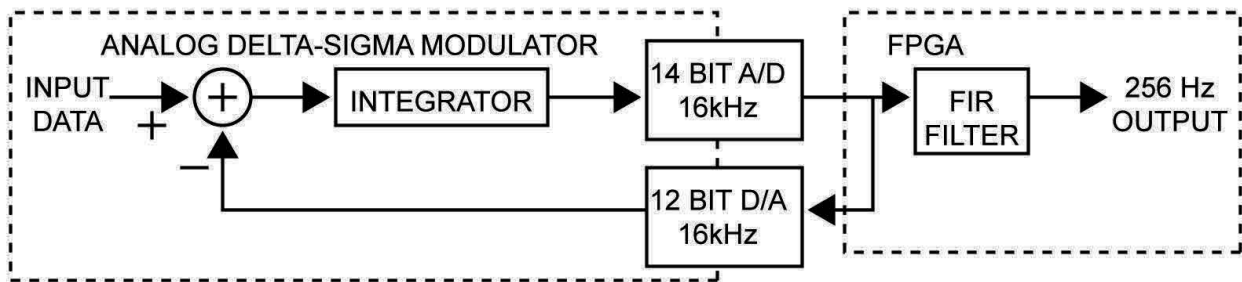
Fig. 1   Block diagram of the delta–sigma analogue-to-digital converter.

2. EXPERIMENTAL METHOD

Figure 2 shows a schematic diagram of the ground experiment to evaluate the non-linearity characteristics of the delta-sigma ADC.   In the flight configuration of MGF, the signal from the sensor (MGF-S) is processed by the analog signal processing circuit in the MGF electronics part (MGF-E) and transferred to the ADC.   For the experiment, the analog signal processing part was temporally disconnected from the ADC. We used a 12V battery and serially connected constant resistance as well as thermistor to input analogue voltage to the ADC.   The input voltage changed continuously by heating and cooling the thermistor.   There were three ranges of the input voltage; high (±5 V), middle (±2.5 V) and low (±1 V), and we changed the range by replacing the constant resistance.   We performed the experiment 5 times for each range for both positive and negative input voltages.   The input voltage was recorded with 1000Hz sampling frequency by a logger in which a 16-bit ADC is implemented.   The recording started by the tick signal provided by MGF-E. The duration of the data recording for each experiment was 65.535 sec.   The output 256Hz data from the ADC were stored in the mission data processor (MDP) emulator through CPU in MGF-E.   The data are recorded together with the interval after the tick signal, which enables us to find the correspondence between the logged input voltage and the output data.
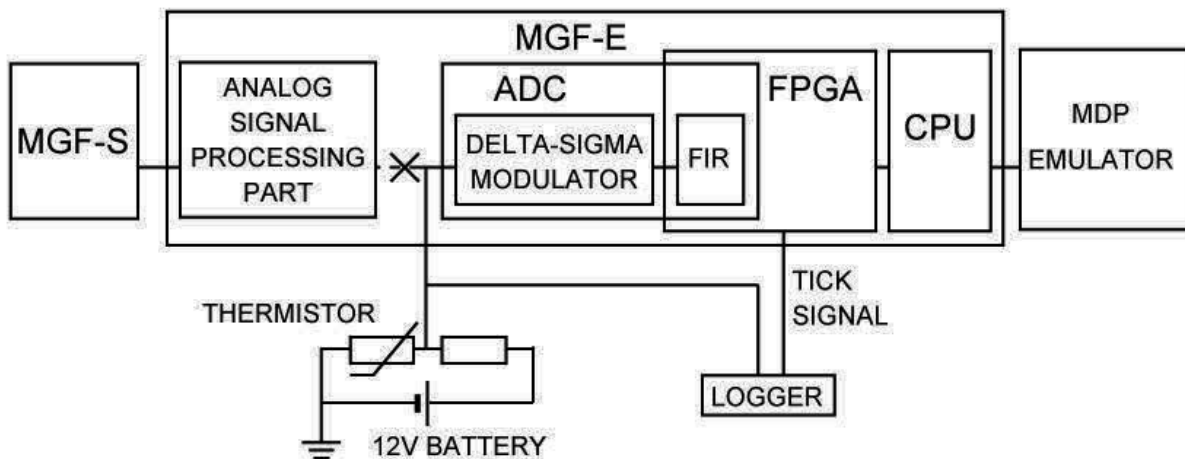

Fig. 2.   Schematic diagram of the experiment to evaluate the non-linearity characteristics of ADC.

3. EVALUATION RESULT

3.1. ADC error versus input voltage
At first the output values from the ADC were fitted to a linear function of the input voltage.   The deviation

of the output values from the regression function was statistically analysed.

Figures 3 shows the devition of the output values versus the input voltage to the (a) x, (b) y and (c) z terminals of the ADC. The deviation of the individual output values is plotted by light-brue dots in the lower panels. The deviation obviously scatters for positive input values of the y and z components. The scattering is considered to be due to the environmental noise although the distinct reason is unclear. The data are divided into bins defined by the input voltage every 5 mV, and the output values are averaged for every bins. The numbers of data in every bins are plotted in the upper panels. The averaged output values are plotted by red and the standard deviation from the average is plotted by dark-blue in the lower panels.

The maximum deviation from the linear relation is 781 digits, 0.07% of the full range, which corresponds to 11 nT (84 nT) for ±8000 nT (±60000 nT) range. The maximum standard deviations from the average of each bin are 103, 80 and 74 digits for negative x, y and z input voltage, respectively, and 89 digits for positive z input voltage. 103 ditits correspond to 1.5 nT (11.0 nT) for ±8000 nT (±60000 nT) measurement range. The standard deviations for positive x and y input voltage are larger, 197 and 213 digits, respectively. 213 digits correspond to 3.1 nT (22.5 nT) for ±8000 nT (±60000 nT) range. By close inspection of the averaged data, the deviation shows steep changes every 0.19 mV of the input voltage. This indicates that the error value steeply changes when the 5th bit from MSB of the output value changes.

3.2. ADC error versus output value

We calibrate the in-flight data of MGF based on the output values, not the input voltage. Therefore we need to know the dependence of the deviation of the output values on the output value itself. Figure 4 shows devition of the output value for the three components again, but the holizontal axis is scaled by the output value. Because the output value has the revese sign to the input voltage, the features seen in Figure 4 are nearly horizontal inversions of those in Figure 3. Statistical bins are newly defined by the output value. As we noted in the last subsection, steep changes occur when the 5th bit from MSB of the output value changes, namely, every 32768 digits. The boundaries of the bins are defined as the factorial of 2, not to mix the data of different 5th bit value. The bin for the x and y components is defined every 1024 digits of the output value, v, for $|v| \geq 2048$ digits, every 8 digits for $-2048 \leq v \leq 256$ digits, every 256 digits for $256 \leq v \leq 2048$ digits. For the z component, it is defined every 1024 digits of v for $|v| \geq 2048$ digits and every 128 digits for $|v| \leq 2048$ digits.

3.3. Application to the MGF calibration

The non-linearity error of ADC presented here cause the inaccuracy of the magnetic field data obtained by Arase MGF. It results in quasi-static error along the spin axis and time variant error in the spin plane. The time variant error has the broad spectrum at frequencies from several hundreds mHz to several Hz. When we need the highly precise field data or study faint field variation in the space, the errors caused by ADC should be serious.

To remove the error by the ADC non-linearity, the deviation shown in Figure 4 is subtracted from the in-flight output values from MGF. The MGF Level-2 data stored in the data sever of ERG Science Center (Miyoshi et al., 2018b) have version numbers corresponding to the calibration method. The ADC non-linearity error is removed from the Level-2 data of version 02 and hereafter.

4. SUMMARY

We performed a ground experiment to evaluate the non-linearity characteristics of the delta-sigma ADC used for Arase MGF. The maximum non-linear error is 781 digits (0.07% of the full range) corresponding to 11 nT (84 nT) for ±8000 nT (±60000 nT) measurement range. The deviation is determined within 103 digits, corresponding to 1.5 nT (11.0 nT) for ±8000 nT (±60000 nT) range, when the environmental interference noise was not intense. It is within 213 digits, corresponding to 3.1 nT (22.5 nT) for ±8000 nT (±60000 nT) range, when the environmental noise was significant.

(a)

(b)

(c)

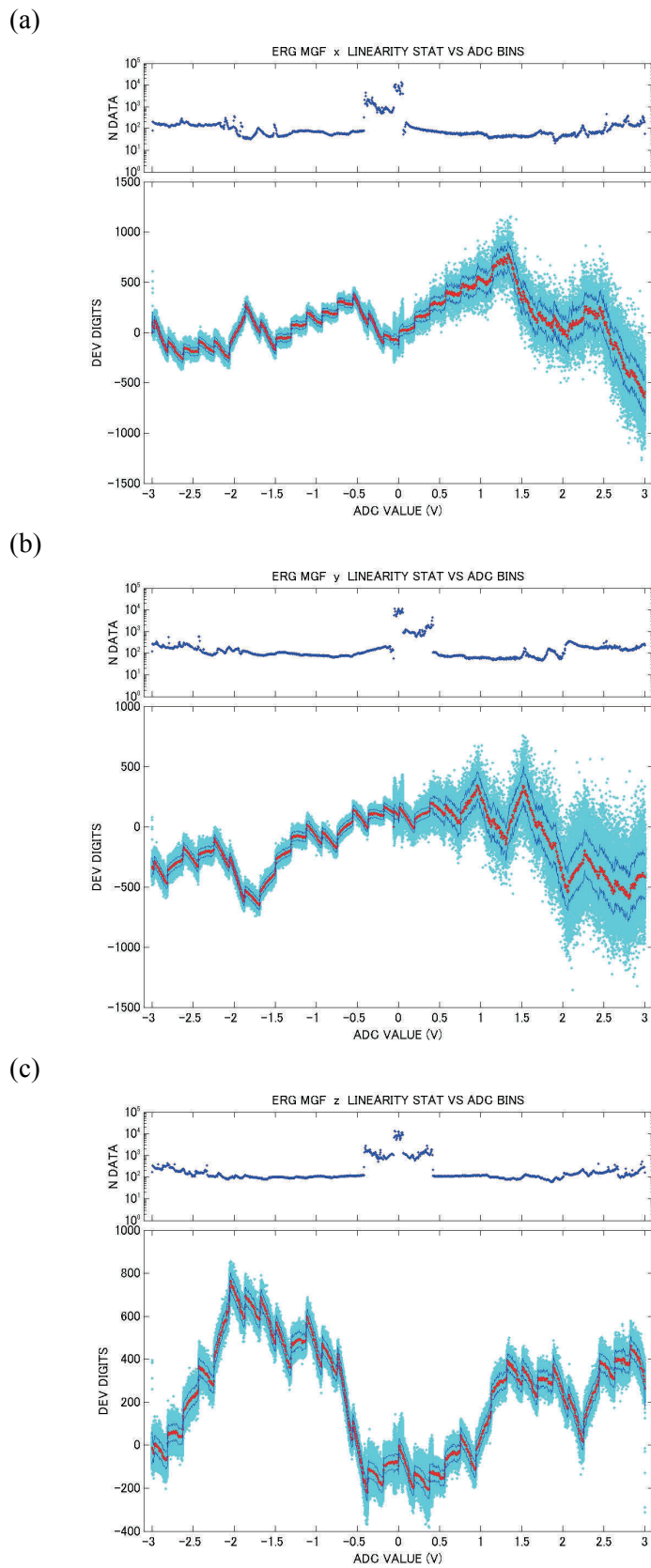

Fig. 3   The devition of the output values versus the input voltage for the (a) x, (b) y and (c) z components.
Light-blue : the deviation of the individual output values, red : the averaged output values for every bins,
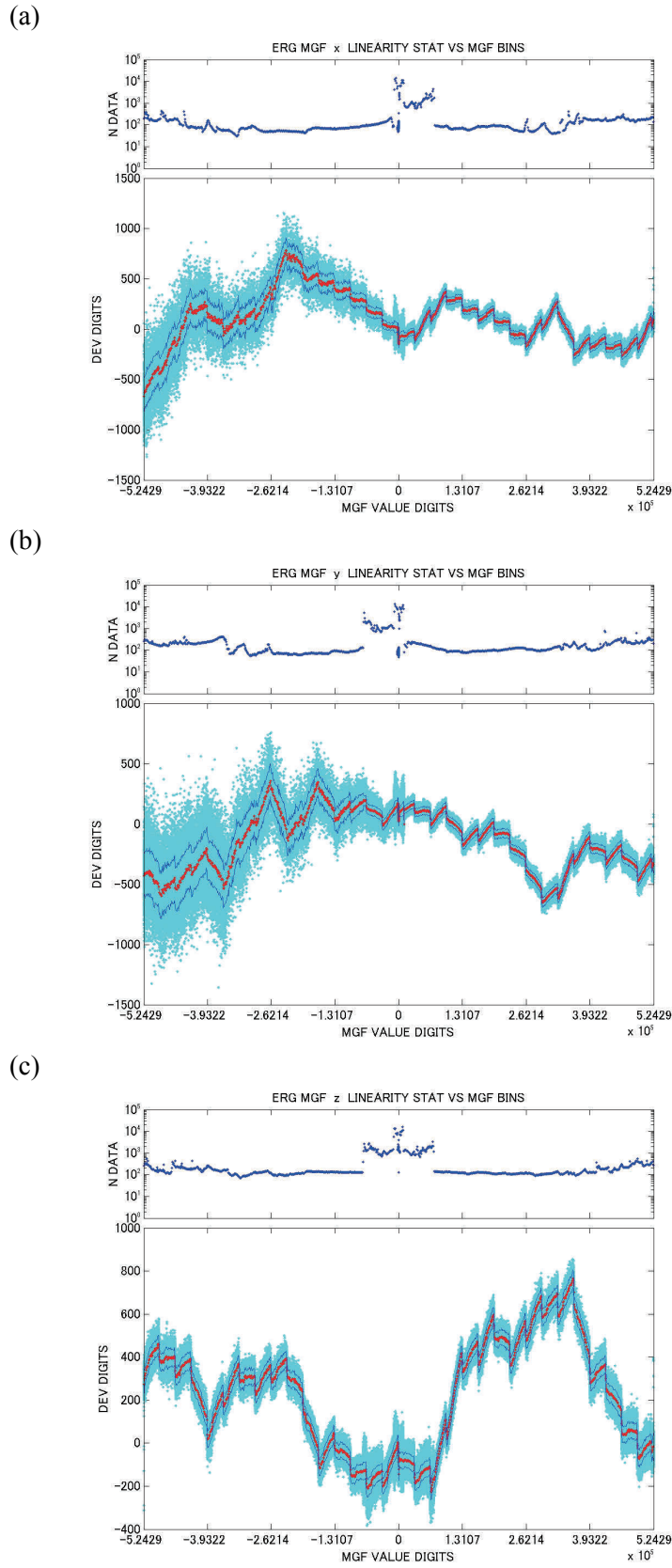dark-blue : the standard deviation from the average for every bins

(a)

(b)

(c)

Fig. 4   The devition of the output values versus the output values for the (a) x, (b) y and (c) z components. The format is same as Fig. 3.

ACKNOWLEDGEMNETS

REFERENCES

Wolfgang Baumjohann, Ayako Matsuoka, Werner Magnes, Karl-Heinz Glassmeier, Rumi Nakamura, Helfried Biernat, Magda Delva, Konrad Schwingenschuh, Tielong Zhang, Hans-Ulrich Auster, Karl-Heinz Fornacon, Ingo Richter, Andre Balogh, Peter Cargill, Chris Carr, Michele Dougherty, Timothy S. Horbury, Elizabeth A. Lucek, Fumio Tohyama, Takao Takahashi, Makoto Tanaka, Tsugunobu Nagai, Hideo Tsunakawa, Masaki Matsushima, Hideaki Kawano, Akimasa Yoshikawa, Hidetoshi Shibuya, Tomoko Nakagawa, Masahiro Hoshino, Yoshimasa Tanaka, Ryuho Kataoka, Brian J. Anderson, Christopher T. Russell, Uwe Motschmann and Manabu Shinohara, Magnetic field investigation of mercury's magnetosphere and the inner heliosphere by MMO/MGF, Planetary and Space Science, 58, 279-286, 2010

Ayako Matsuoka, Mariko Teramoto, Reiko Nomura, Masahito Nosé, Akiko Fujimoto, Yoshimasa Tanaka, Manabu Shinohara, Tsutomu Nagatsuma, Kazuo Shiokawa, Yuki Obana, Yoshizumi Miyoshi, Makoto Mita, Takeshi Takashima and Iku Shinohara, The ARASE (ERG) magnetic field investigation, Earth, Planets and Space, 70:43, 10.1186/s40623-018-0800-1, 2018

Miyoshi, Y., I. Shinohara,, T. Takashima, K. Asamura, N. Higashio, T. Mitani, S. Kasahara, S. Yokota, Y. Kazama, S.-Y. Wang, S. W. Tam, P. T. P Ho, Y. Kasahara, Y. Kasaba, S. Yagitani, A. Matsuoka, H. Kojima, H. Katoh, K. Shiokawa, and K. Seki, Geospace Exploration Project ERG, Earth Planets Space, 10.1186/s40623-018-0862-0, 2018a

Miyoshi, Y., T. Hori, M. Shoji, M. Teramoto, T. F. Chang, S. Matsuda, S. Kurita, T. Segawa, N. Umemura, K. Keika, Y. Miyashita, Y. Tanaka, N. Nishitani, T. Takashima, and I. Shinohara, The ERG Science Center, Earth, Planets and Space, 10.1186/s40623-018-0867-8, 2018b

In-orbit Alignment Analysis of the Magnetometer Sensor on the Arase (ERG) Satellite

Ayako MATSUOKA[*1], Mariko TERAMOTO [*2], Reiko NOMURA [*3]

ABSTRACT

Precise magnetic field measurement is aimed in the Arase project to investigate the growth and decline of the earth radiation belt.　The sensing directions of the magnetometer sensor elements in the spacecraft reference frame are calculated by the analysis of the in-orbit magnetic field data.　They are determined with good accuracies, within 0.05° and 0.2° for the ±8000 nT and ±60000 nT measurement ranges, respectively. The misalignment angles are continuously varying with the time, and the variation is supposed to be caused by the mechanical deformation of the extendable MAST on which the magnetometer sensor is mounted.

Keywords: Arase, ERG, MGF, magnetometer, calibration, alignment

1. INTRODUCTION

Many magnetometers have boarded on the spacecraft and measured the magnetic fields in the space.　The accurate measurement of the magnetic field direction is essential for several scientific objectives, i.e., pitch angle determination of the charged particles and examination of the high-order components in the planetary magnetic moment.

To precisely measure the magnetic field direction, we need to accurately determine the sensing directions of the sensor elements in the spacecraft reference frame as well as the spacecraft attitude in the inertia coordinate. When the spacecraft is spinning, knowledge of the sensor alignment in the spacecraft reference frame is also necessary for accurate determination of the measurement offset.

When the sensor is mounted on a deployment boom, the sensor alignment may change over time due to the deformation of the boom.　Therefore the sensor alignment in the spacecraft reference frame is difficult to determine in advance in the ground experiments. Meanwhile, in the case of spinning spacecraft, the inclination angles of the sensor can be calculated from the amplitude and phase of the sinusoidal wave forms in the in-orbit data, if the sensitivity of the sensor elements are precisely calibrated and the magnetic field is sufficiently stable during the spin period.

Arase (also known as Energization and Radiation in Geospace, ERG) is a satellite orbiting around the earth to study the generation and loss mechanism of relativistic electrons in the radiation belts (Miyoshi et al., 2018). A magnetometer, Magnetic Field Experiment (MGF), is installed in the Arase satellite for the precise measurement of the magnetic field.　The design and characteristics of MGF are described in Matsuoka et al. (2018).　We evaluated the MGF sensor alignment in the spacecraft reference frame.

2. ANALYSIS METHOD

Figure 1 shows the photo of the MGF sensor unit.　Three sensor elements, X, Y and Z are mounted on the sensor base to measure the three orthogonal components of the magnetic field.　The angles between the sensing directions of the three sensor elements are very close to 90° and determined in the ground experiment (Teramoto et al., 2018).　The sensor Z is nearly parelle to the spacecraft spin axis.

Figure 2 (a) shows the definition of an intermediate coordinate O_1 to determine the sensor alignment angles in the spacecraft reference frame. O_1 is defined as an orthogonal coordinate that has the same X-direction and coplanar X–Y with the sensor. Figure 2 (b) shows the relationship between O_1 and the spin coordinate which has the Z direction along the spacecraft spin axis and coplanar X–Z with the sensor. Sensor misalignment is expressed by inclination angles α and β of O_1 in the spin coordinate.
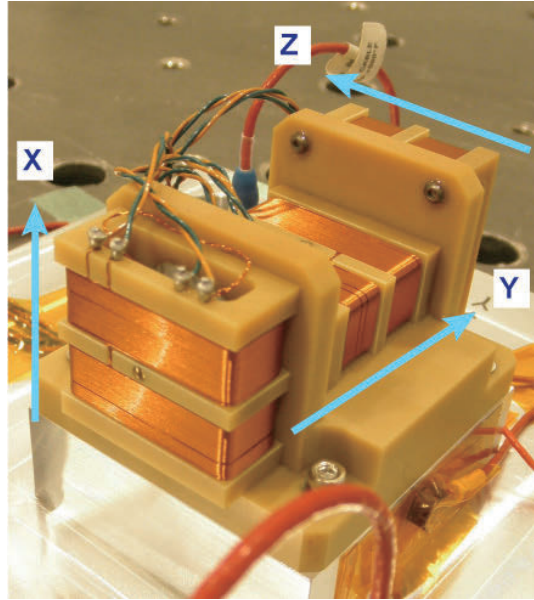
Fig. 1   Photo of the MGF sensor unit.   Three sensor elements, X, Y and Z are mounted on the sensor base.
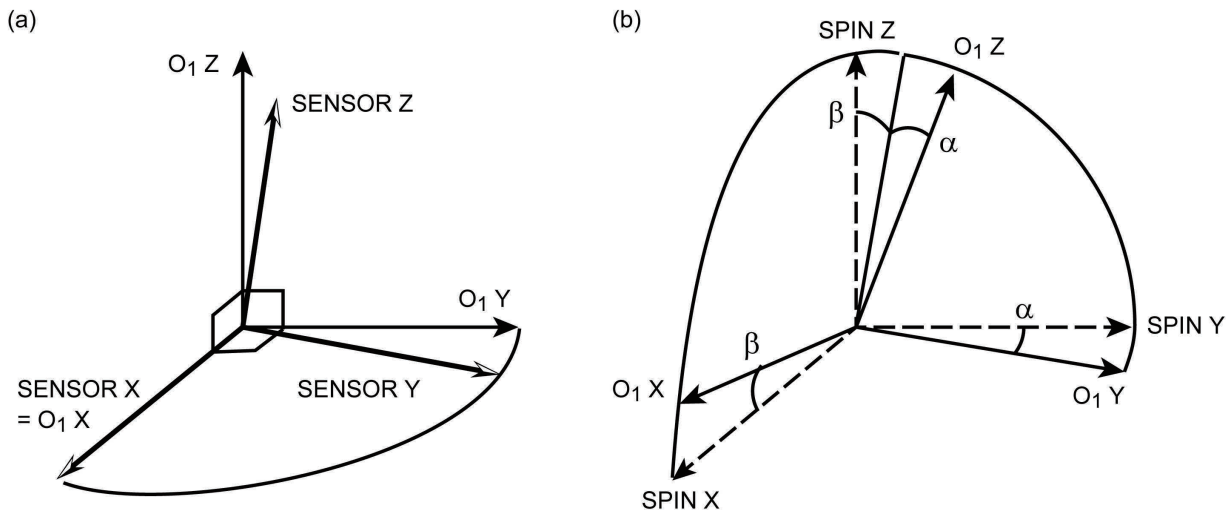
Fig. 2   Relationship between the sensor non-orthogonal coordinate and the spacecraft reference frame, as well as the definitions of the misalignment angles, α and β. (a) An intermediate orthogonal coordinate O_1 is defined to have the same X-direction and coplanar X–Y with the sensor. (b) The sensor misalignment is expressed by inclination angles α and β of O_1 in the reference coordinate with respect to the spacecraft spin axis.
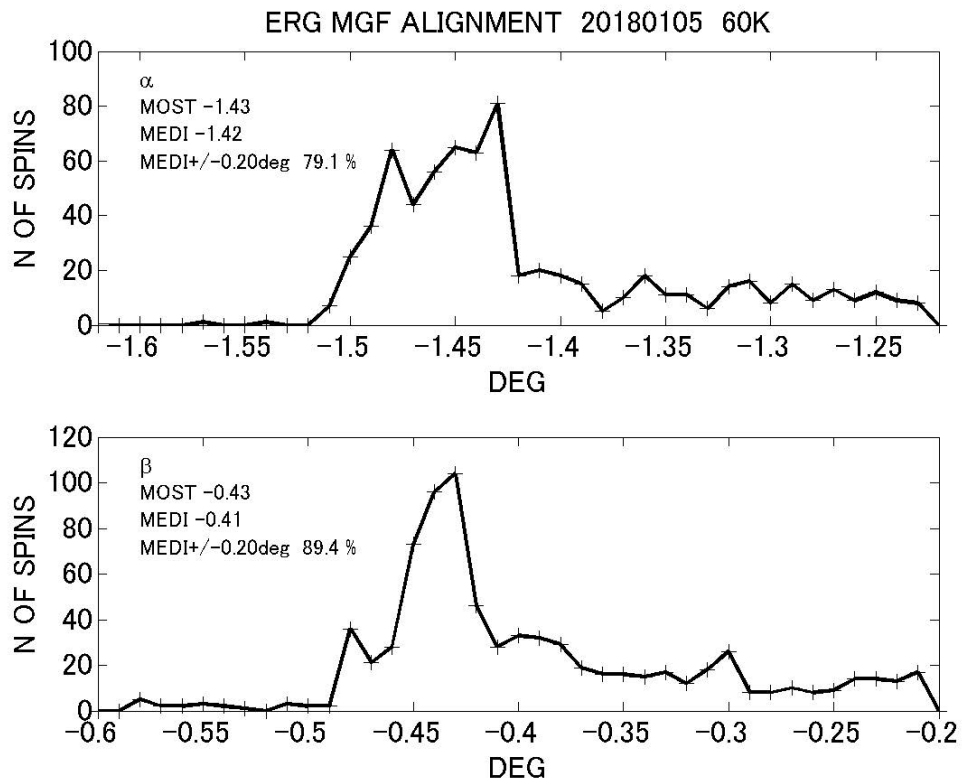
(a)
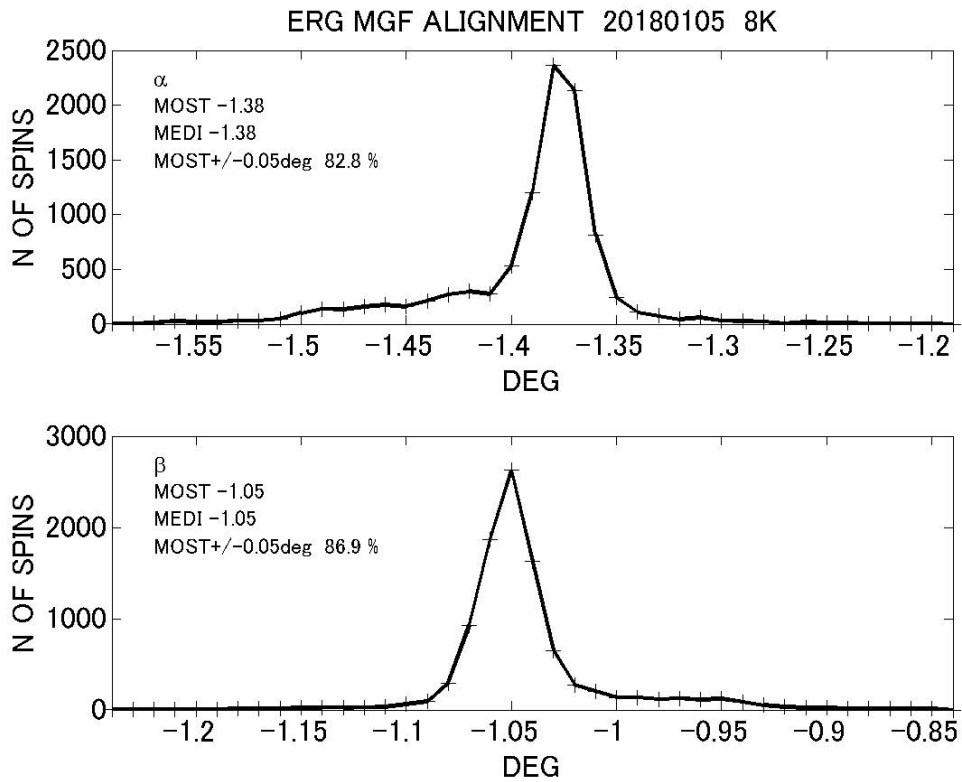
(b)

Fig. 3   Statistical results for the sensor misalignment angles α and β on January 5, 2018 for the measurement ranges (a) ±8000 nT and (b) ±60000 nT.

In the frame of a rotating spacecraft, the magnetic field in the spin plane varies simusoidally with the same period as the rotation, while the magnetic field along the spin axis is static. The output signals from the three sensor elements are the projections of the magnetic field to the sensing directions in the spacecraft frame. The amplitude and phase of the simusoidal waves in the output signal reflect the inclination and azimth angles of the sensing directions in the spacecraft frame. Namely, α and β in Figure 2 (b) can be expressed by the amplitude and phase of the output sinusoidal signal from the three sensor elements. Details about the computation method are described in a separated report (Matsuoka et al., 2019).

3. RESULTS

3.1. Daily Statistics of the Misalignment Angles

We calculated the misalignment angles α and β for every spacecraft rotations and took the daily statistics. Matsuoka et al. (2018) showed an example of the statistics on March 19, 2017. Here we show another example on January 5, 2018. Figure 3 shows the distributions of the sensor misalignment angles. For the ±8000 nT measurement range, the distribution of α (β) exhibited a clear peak at −1.38° (−1.05°) (Figure 3 (a)), and 83% (87%) of the α (β) samples were within ±0.05° of the peak. For the ±60000 nT measurement range, the distribution was broader (Figure 3 (b)), and 79% (89%) of the α (β) samples were within ±0.20° of the median value of −1.42° (−0.41°). We note that the field intensity changes rapidly near the perigees, where the measurement range is nominally ±60000 nT. Time variation of the field intensity during a spin period could cause errors and broadening of the distribution of the calculated misalignment angle.

The misalignment angles are difference between two ranges, ±8000 nT and ±60000 nT. The difference is 0.16° for α and 0.64° for β. The difference is meaningful even we consider the large statistical errors for the ±60000 nT. There would be several possible reasons which cause the difference. The major one is the difference of the inter-axes alignment angles we derived in the ground experiment. The sensor alignment angles in the reference frame defined by the cubic mirror are different between the two ranges, ±8000 nT and ±60000 nT (Teramoto et al., 2018). The difference is about 0.6° and very similar to the difference shown here.
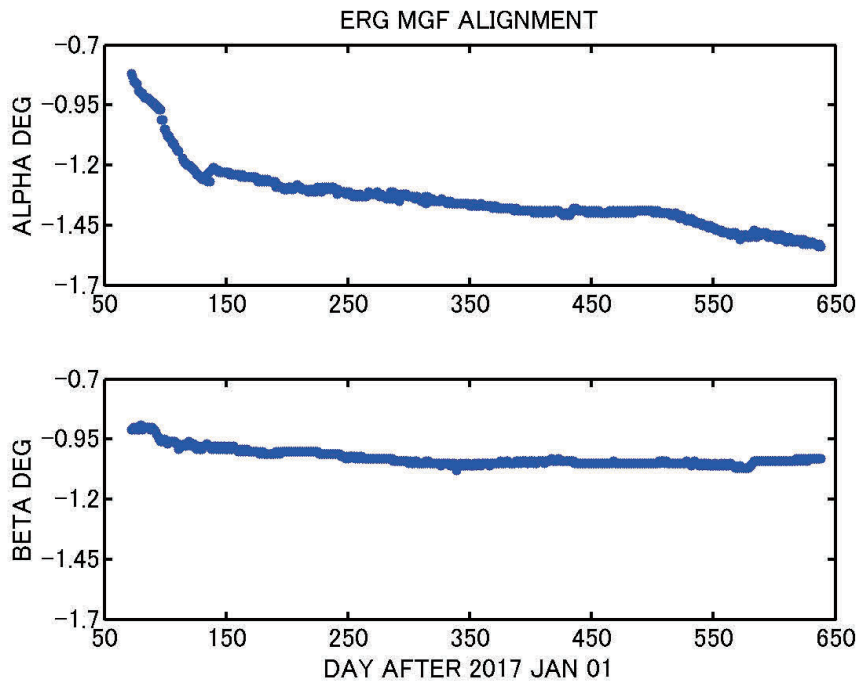

Fig. 4 Time variation of misalignment angles α (upper panel) and β (lower panel) for the ±8000 nT measurement range from March 13 2017 to September 30 2018.

3.2. Time Variation of the Misalignment Angles

Figure 4 shows the time variation of the misalignment angles α and β for the ±8000 nT measurement range from March 13 2017 to September 30 2018.   Both show a general tendency to decrease with the time.   The changing speed of α, roughly $-6.5°\times10^{-4}$/day, is faster than that of β, $-1.0°\times10^{-4}$/day.   It may be interpreted that the time vation of the misalignment angles would be caused by the mechanical relaxation of the extendable 5-m MAST on which the MGF sensor is mounted.   Figure 5 shows the Arase spacecraft configuration after the deployment of the MAST and correspondence with α and β. α is defined as the rotation of the MAST around the deployment direction while β corresponds to the inclination from the spacecraft spin plane.   The MAST deployment operation was performed on January 17, 2017.   During the deployment the tip of the MAST rotated counterclockwise when viewing from the spacecraft $-y$ (deployment direction).   The long-term negative vatiation of α seen in Figure 4 indicates that the MAST is slowly rotating in the same direction.

Figure 4 shows that the changes of α and β are not very monotonic and the changing speeds are not uniform. The irregular variation of α on the days 130–140 especially draws our attension.   It is not easy to interpret such irregular variations because the long-period stability of the MAST shape is not examined in the ground experiment.
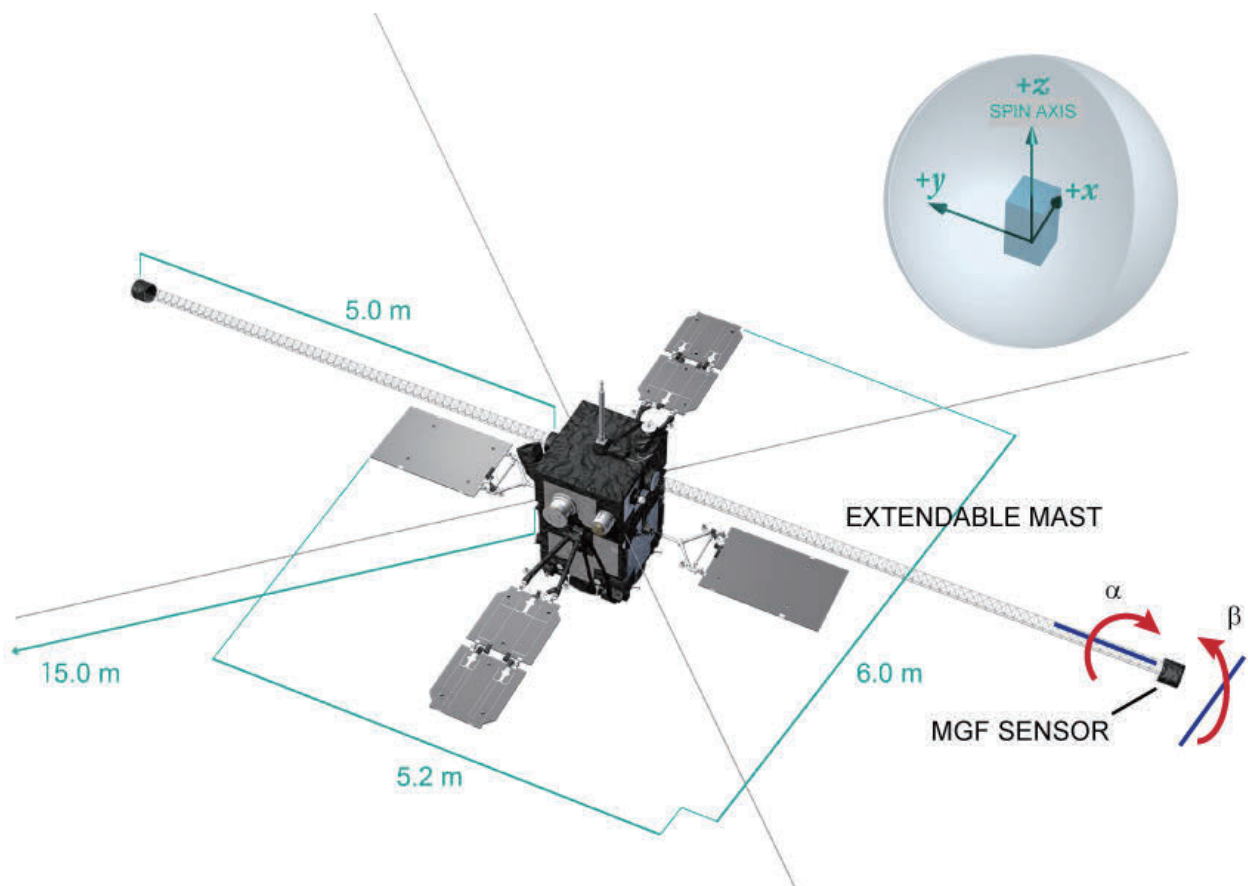

Fig. 5   Arase spacecraft configuration after the deployment of MAST and correspondence with the α and β.

4. SUMMARY

We analyzed the in-orbit Arase MGF data and calcurated the sensing directions of the.three sensor elements in the reference frame defined by the spacecraft spin axis.   The alignment angles are determined with better accuracy than 0.05° and 0.2° for the ±8000 nT and ±60000 nT measurement ranges, respectively.   These angular accuracies are enoght to calibrate the in-orbit MGF data with the finally aimed acuracy.

The alignment angles have continuously varied with time for one year and seven months after starting of the regular measurement.   The variation is consistent with the rotation of the sensor accompanied by the mechanical relaxation of the MAST.

REFERENCES

Ayako Matsuoka, Mariko Teramoto, Reiko Nomura, Masahito Nosé, Akiko Fujimoto, Yoshimasa Tanaka, Manabu Shinohara, Tsutomu Nagatsuma, Kazuo Shiokawa, Yuki Obana, Yoshizumi Miyoshi, Makoto Mita, Takeshi Takashima and Iku Shinohara, The ARASE (ERG) magnetic field investigation, Earth, Planets and Space, 70:43, 10.1186/s40623-018-0800-1, 2018

Ayako Matsuoka, Mariko Teramoto and Reiko Nomura, Method to Determine the In-orbit Sensor Alignment of the Magnetometer Onboard a Spin-stabilized Satellite(Japanese), JAXA Research and Development Memorandum, JAXA-RM-18-008, 10.20637/JAXA-RM-18-008/0001, 2019

Miyoshi, Y., I. Shinohara,, T. Takashima, K. Asamura, N. Higashio, T. Mitani, S. Kasahara, S. Yokota, Y. Kazama, S.-Y. Wang, S. W. Tam, P. T. P Ho, Y. Kasahara, Y. Kasaba, S. Yagitani, A. Matsuoka, H. Kojima, H. Katoh, K. Shiokawa, and K. Seki, Geospace Exploration Project ERG, Earth Planets Space, 2018a

Mariko Teramoto , Ayako Matsuoka and Reiko Nomura, Re-evaluation of the ground calibration for the Arase Magnetic Field Experiment, JAXA Research and Development Report, JAXA-RR-18-005E, 10.20637/JAXA-RR-18-005E/0001, 2019

あらせ衛星/MGF センサにおける人工衛星起因の直流成分磁場ノイズ
(1) Tsyganenko 89 モデルを用いた評価

山本 和弘[*1]，生松 聡[*1]，能勢 正仁[*2]，
松岡 彩子[*3]，寺本 万里子[*2]，今城 峻[*2]

DC component of spacecraft-origin magnetic field noise
at the Arase/MGF sensor: (1) Evaluation with Tsyganenko 89 model

Kazuhiro YAMAMOTO[*1], Satoshi OIMATSU[*1], Masahito NOSÉ[*2], Ayako MATSUOKA[*3],
Mariko TERAMOTO[*2], Shun IMAJO[*2]

ABSTRACT

We investigated the difference between the magnetic field observed by the Arase spacecraft and the Tsyganenko 89 model field (ΔB) during geomagnetic quiet period to determine the DC component of spacecraft-origin magnetic field noise at the position of Magnetic Field Experiment (MGF) onboard the Arase spacecraft. The median value of the Z-component of ΔB in the Despun Sun sector Inertia (DSI) coordinates is very small (-0.6 nT); therefore, MGF has a good magnetic field cleanness and is well-calibrated. We also found that the Z-component of the magnetic field in the SM coordinate system observed by Arase is usually larger than that of the model field by ~3 nT. The difference between time periods for the data used in this study and for the data to create the Tsyganenko 89 model may cause the discrepancy.

1. INTRODUCTION

The Arase spacecraft measures three dimensional velocity distributions of electrons and ions with a wide energy range to study wave-particle interactions. The accurate measurement of the electromagnetic field is important for this objective. The sensitivity and offset of Magnetic Field Experiment (MGF) onboard the Arase have already been evaluated in the ground calibration (Teramoto et al., 2017[1]; Matsuoka et al., 2018[2]). It was found that the magnetic field offset depends on temperature and its variation between -20 and 30 ℃ is less than 5 nT, which meets a requirement for MGF measurement of the magnetic field strength (Teramoto et al., 2017[1]). Although the MGF instrument is equipped at the end of 5-m MAST to minimize contamination by spacecraft-origin magnetic field noises, the contamination during the satellite operation is not yet evaluated. In addition, in-flight temperature drift of the offset and inaccuracy of spacecraft attitude also cause some errors in magnetic field measurement.

The MGF is a fluxgate magnetometer composed of three orthogonal sensor elements. The X and Y elements are almost perpendicular to the spin axis of the spacecraft. The in-flight offsets and the stray field for X and Y elements can be determined from a sinusoidal waveform of the magnetic field due to the spin of the spacecraft. If the Earth's main field do not vary significantly in one spacecraft rotation (~7.98 s), the magnetic field measured by X/Y element will oscillate between $B_0 \cos\theta + B_{Noise}$ and $-B_0 \cos\theta + B_{Noise}$, where B_0 is the background magnetic field, θ is an angle between B_0 and the direction of the X/Y element, and B_{Noise} is the artificial magnetic noises including the magnetic field offset and the spacecraft-origin magnetic field noise. Thus the DC components of the magnetic field variation reflect these noises. This evaluation of the noises is performed in the process of the scientific data creation, and the noises for X and Y elements are corrected.

Regarding the *Z* element, however, we cannot evaluate the noises in the same method, because the *Z* element almost directs to the spin axis. Since the temperature used for calibration of offset of the *Z* element is fixed at specific temperature, there is also an estimation error of the offset for the *Z* element. In this study, therefore, we statistically compare the magnetic field observed by the *Z* element with the Tsyganenko 89 (T89) model field (Tsyganenko, 1989[3]) during geomagnetic quiet period, and evaluate the spacecraft-origin magnetic field noise and the estimation error of the offset on the *Z* element measurement.

(a) Histogram of ΔBz (Arase - T89, 8K)
Kp ≤ 0.3, |dB|/dt/Bt ≤ 0.006 [/7.98s]

Most Frequent Value: -0.1 [nT]
Average Value: -0.3 [nT]
Median Value: -0.6 [nT]
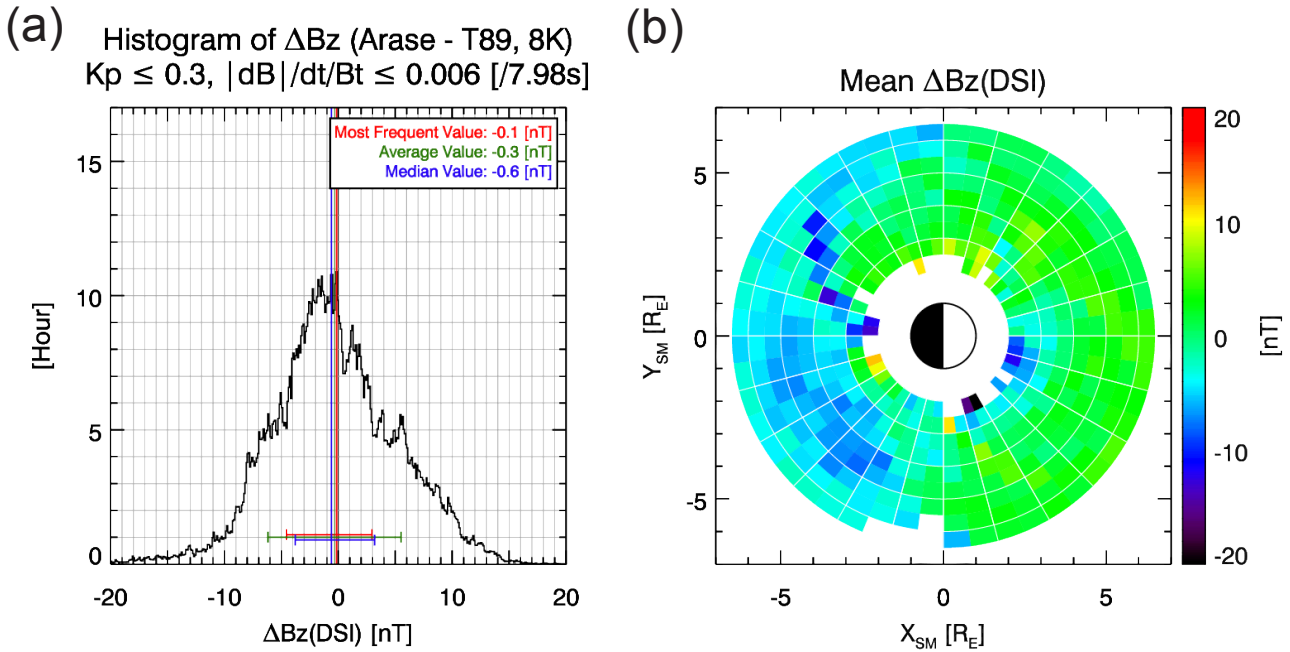
(b) Mean ΔBz(DSI)

Figure 1 (a) Histogram of the difference of $B_{Z,DSI}$ between the Arase/MGF observation and the T89 model field. The vertical lines represent the most frequent value (red), the average value (green), and the median value (blue). The horizontal error bars show the full width of the half maximum (red), the standard deviation (green), and the first and third quartiles (blue). **(b)** R-MLT distribution of the averaged $\Delta B_{Z,DSI}$ in the SM coordinate system.

2. ANALYSIS

2.1. Data Selection

We used the spin-averaged magnetic field data (v01.01) obtained by MGF from 23rd March 2017 to 30th April 2018. In this version, the data are calibrated for the sensitivity of MGF sensor using the temperature on the orbit, and for the miss alignment due to the twisting MAST. The offset of the *Z* element is estimated at a specific temperature from the results of the ground calibration, and the offset is subtracted from observed values.

We analyzed the data during geomagnetic quiet period to avoid a large difference between the observed magnetic field and the model field (ΔB) due to natural signals like dipolarization during substorms. The quiet periods were defined as intervals when the Kp index was 0o or 0+. We found about 1320 hours (55 days) of such period.

The MGF instrument has two dynamic ranges: ±8,000 nT range and ±60,000 nT range. MGF measures the magnetic field with ±60,000 nT dynamic range near the Earth, but we excluded the ±60,000 nT range data from our analysis because the determination error of the absolute sensitivity for the ±60,000 nT range is too large (0.1 %) to evaluate the relatively small magnetic field noises. We imposed another criterion: $\Delta B_{1-spin}/Bt <$ 0.006, where ΔB_{1-spin} is the magnetic field variation in one spin period and *Bt* is the total intensity of the magnetic field. This is because $|\Delta B|$ rapidly increases when $\Delta B_{1-spin}/Bt$ is greater than 0.006.

From 1st October 2017 to 3rd November 2017, the algorithm for changing the dynamic range did not work well. Hence we did not examined this data period. Spike noises sometimes appear in the magnetic field data, and we removed them before the analysis.

2.2. Comparison with Tsyganenko 89 Model

After choosing the data during the geomagnetic quiet period, we calculated the model field values by using the T89 model. In the calculation, the Kp index was fixed at Kp = 0 to express the ground state of the magnetosphere. We compared the observed magnetic field with the model field in the Despun Sun sector Inertia (DSI) coordinate system. In this coordinate system, Z axis (Z_{DSI}) almost directs to the spin axis. Since the angle between Z_{DSI} and the spin axis is less than 1 degree, we can consider the Z-component of the magnetic field in the DSI coordinates ($B_{Z,DSI}$) as the magnetic field observed by the Z sensor element. Our final goal is to evaluate the difference in $B_{Z,DSI}$ between the spacecraft observation and the T89 model field ($\Delta B_{Z,DSI}$).

The Arase spacecraft has an apogee altitude of ~32,000 km and a perigee altitude of ~440 km (Miyoshi et al., 2018[4]). Since Arase's apogee precesses 270 degree per year, we can examine $\Delta B_{Z,DSI}$ at various radial distances (R) and magnetic local time (MLT). Arase's observation covers almost all MLT during the data period used in this study.

3. RESULTS

3.1. Histogram and R-MLT Distribution of the $\Delta B_{Z,DSI}$

Figure 1a shows the histogram of $\Delta B_{Z,DSI}$ for the selected data period. Note that this histogram is strongly biased by the values around the apogee of Arase, because Arase was launched into elliptical orbit and the spacecraft spends much time around the apogee. Since the magnetic field noise originated from spacecraft should not vary with radial distances or MLT, it is appropriate for evaluation of the noise to use all period of the data. The most frequent value of $\Delta B_{Z,DSI}$ is -0.1 nT, the average value is -0.3 nT, and the median value is -0.6 nT. These values are much smaller than the offset of Z sensor element determined in the ground calibration (from -10 to -13 nT, Teramoto et al., 2017[1]). The histogram shows variance that may be created by weak geomagnetic disturbance. It seems that there are some local peaks around the maximum of the occurrence frequency in the histogram. Thus the median value is better than the other values to evaluate the noises. Figure 1b shows the radial distance vs MLT distribution of $\Delta B_{Z,DSI}$ in a XY plane of the SM coordinate system. We found that $\Delta B_{Z,DSI}$ depends on MLT; that is, $\Delta B_{Z,DSI}$ is positive on the dayside while it is negative on the nightside.
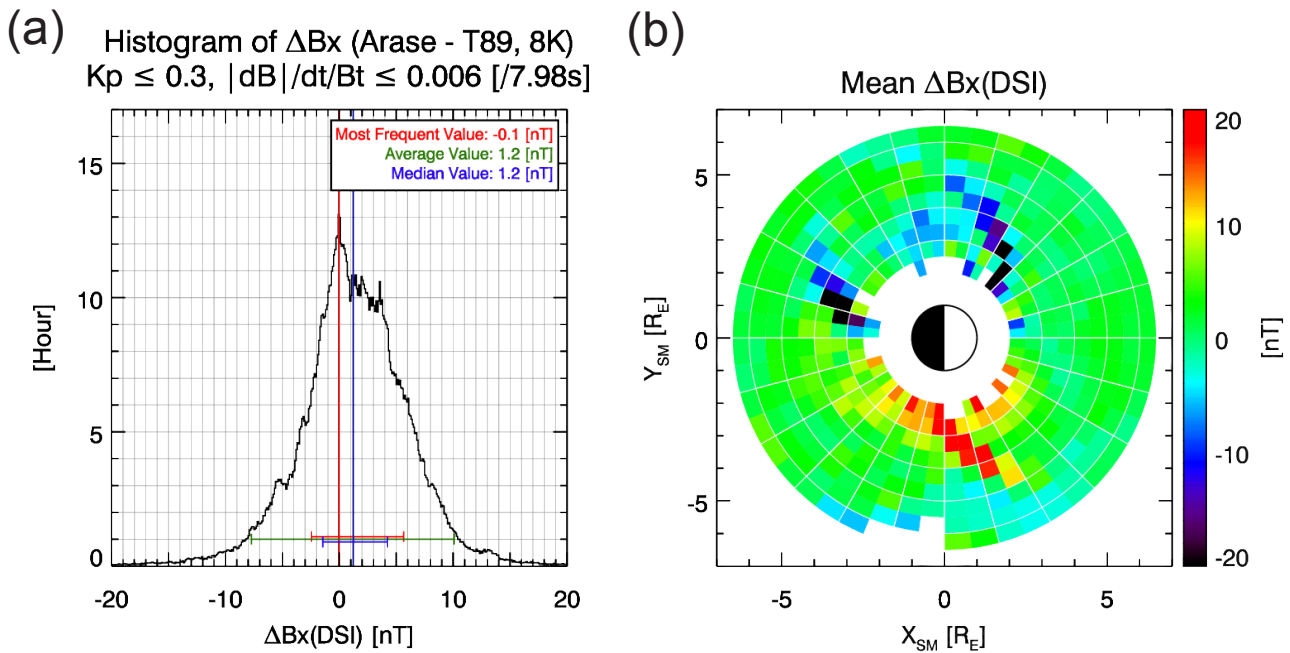

Figure 2 (a) Same as Figure 1a but for $\Delta B_{X,DSI}$. **(b)** Same as Figure 1b but for $\Delta B_{X,DSI}$.

3.2. Histogram and R-MLT Distribution of the $\Delta B_{X,DSI}$ and $\Delta B_{Y,DSI}$

We also examined the differences between the observed magnetic field and the model field for X and Y components in the DSI coordinate system ($\Delta B_{X,DSI}$ and $\Delta B_{Y,DSI}$). The results are shown in Figures 2 and 3. As for $\Delta B_{X,DSI}$, the median value is slightly large (+1.2 nT) and variance of $\Delta B_{X,DSI}$ seems more small than that of $\Delta B_{Z,DSI}$. $\Delta B_{X,DSI}$ has no clear radial or local time dependence, and is usually positive (Figure 2b). The $\Delta B_{Y,DSI}$ is the largest among the three components. The median value is 3.1 nT and the histogram has large variance (Figure 3a). $\Delta B_{Y,DSI}$ also has no radial or local time dependence as shown in Figure 3b.
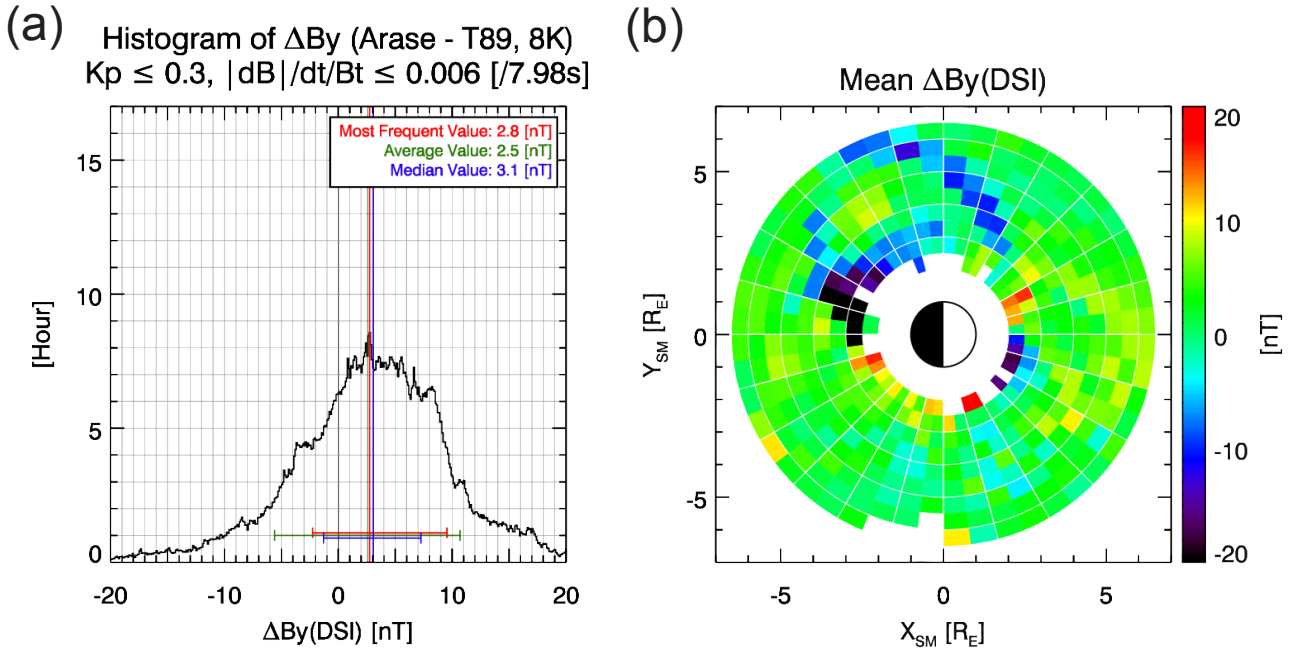
Figure 3 (a) Same as Figure 1a but for $\Delta B_{Y,DSI}$. **(b)** Same as Figure 1b but for $\Delta B_{Y,DSI}$.

4. SUMMARY and DISCUSSION

4.1. Spacecraft-origin Noise and Estimation Error of the Offset in the Z Sensor Element

We compared the magnetic field observed by the Arase with the T89 model in the DSI coordinates during geomagnetic quiet period, and the result is summarized in Table 1. We cannot distinguish if these differences are caused by estimation errors of the sensor offset, the DC component of the spacecraft-origin magnetic field noise or the inaccuracy of the T89 model, because observational errors due to these factors can have similar values as discussed below. According to Teramoto et al. (2017)[1], the temperature drift of the offset for the Z element sensor is -0.1 nT/℃ around 0 ℃. Therefore, the estimation error of the offset can be comparable to $|\Delta B_{Z,DSI}|$ for different temperatures between in the offset estimation and in flight. The spacecraft-origin magnetic field noise at the tip of the MAST has been simulated by Matsuoka et al. (2017)[2], and they found that the turned-off spacecraft creates the spacecraft-origin noise by 0.18 nT. This value is also comparable to $|\Delta B_{Z,DSI}|$. The inaccuracy of the T89 model during the quiet period may be less than ~1 nT and can contribute to $\Delta B_{Z,DSI}$. Nevertheless, the total influence of the artificial noises on the magnetic field measurement by the Z element may be very small (within ±1 nT) and the MGF sensor measures the magnetic field with high accuracy.

The clear MLT dependence of $\Delta B_{Z,DSI}$ can be attributed to the inaccuracy of the MGF sensitivity or the T89 model, because the estimation error of the offset and the spacecraft-origin magnetic field noise should be independent on MLT. As a definition of the DSI coordinates, Z_{DSI} roughly directs to tailward. Since the Arase stays in the northern hemisphere for longer time than in the southern hemisphere (not shown), the positive $\Delta B_{Z,DSI}$ on the dayside and the negative one on the nightside imply that the main field is stronger than that assumed in the T89 model. The error in the sensitivity is too small (0.06% for ±8,000 nT range) to explain the large differences (> 1 nT). Therefore, we consider that the T89 model may underestimate the main field.

Table 1 Differences between the magnetic field observed by the Arase spacecraft and the T89 model field in the DSI coordinate system during geomagnetic quiet period

	Most Frequent Value [nT]	Average Value [nT]	Median Value [nT]
$\Delta B_{X,DSI}$	-0.1	1.2	1.2
$\Delta B_{Y,DSI}$	2.8	2.5	3.1
$\Delta B_{Z,DSI}$	-0.1	-0.3	-0.6

4.2. Interpretation of the large $\Delta B_{Y,DSI}$

As shown in Table 1, $\Delta B_{Y,DSI}$ is the largest among the three components. To understand the reason for the large difference in $B_{Y,DSI}$, we investigated the direction of Y_{DSI} in the SM coordinates. Figure 4 shows the dwelling time of Arase as well as the three components of the unit vector along the Y_{DSI} axis in the SM coordinates. We can see that the Y_{DSI} axis approximately directs to the Z_{SM} axis except for the dusk sector. Therefore, the large $\Delta B_{Y,DSI}$ may be due to the underestimation of the magnetic field in Z_{SM} ($B_{Z,SM}$) by the T89 model. The magnetic field observed by Arase is closer to the dipole field than the model field.

Some possible reasons for the underestimation of $B_{Z,SM}$ can be considered. Since the Arase's data period covers only the declining phase of the solar activity or the solar minimum, the magnetopause current may be weaker than that assumed in the T89 model. Thus the magnetic field induced by the magnetopause current along the main field should be small, and the main field will be larger than that expected in the T89 model. The other possible reason is the secular variation of the main field. Since the T89 model was coded about 30 years ago, the model field assumes stronger internal magnetic field than the data period used in this study. This may causes some errors in the estimation of parameters for an external field induced by magnetospheric current system.
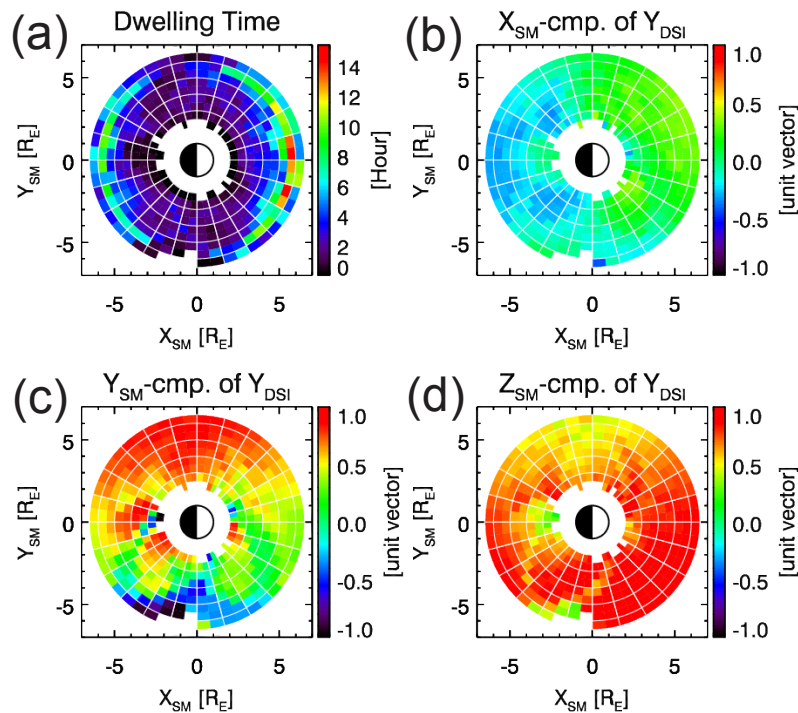

Figure 4 (a) Dwelling time of the Arase spacecraft in XY plane of the SM coordinates. **(b)** X-component of the unit vector of Y_{DSI} axis. **(c)** Y-component of the unit vector of Y_{DSI} axis. **(d)** Z-component of the unit vector of Y_{DSI} axis.

REFERENCES

[1] Teramoto M, Matsuoka A, Nomura R (2017) Ground calibration experiments of Magnetic field experiment on the ERG satellite (Japanese). *JAXA Research and Development Memorandum* JAXA-RM-16-003

[2] Matsuoka, A., Teramoto, M., Nomura, R., Nosé, M., Fujimoto, A., Tanaka, Y., Shinohara, M., Nagatsuma, T., Shiokawa, K., Obana, Y. and Miyoshi, Y. (2018). The ARASE (ERG) magnetic field investigation. *Earth, Planets and Space*, 70(1), 43.

[3] Tsyganenko, N. A. (1989). A magnetospheric magnetic field model with a warped tail current sheet. *Planetary and Space Science*, *37*(1), 5-20.

[4] Miyoshi, Y., I. Shinohara, T. Takashima, K. Asamura, N. Higashio, T. Mitani, S. Kasahara, S. Yokota, Y. Kazama, S.-Y. Wang, S. W. Tam, P. T. P Ho, Y. Kasahara, Y. Kasaba, S. Yagitani, A. Matsuoka, H. Kojima, H. Katoh, K. Shiokawa, K. Seki (2018), Geospace Exploration Project ERG, *Earth, Planets and Space*, doi:10.1186/s40623-018-0862-0.

あらせ衛星/MGF センサにおける人工衛星起因の直流成分磁場ノイズ

(2) Tsyganenko-Sitnov 04 モデルを用いた評価

生松 聡[*1]，山本 和弘[*1]，能勢 正仁[*2]，松岡 彩子[*3]，寺本 万里子[*2]，今城 峻[*2]

DC component of spacecraft-origin magnetic field noise at the Arase/MGF sensor: (2) Evaluation with Tsyganenko-Sitnov 04 model

Satoshi OIMATSU[*1], Kazuhiro YAMAMOTO[*1], Masahito NOSÉ[*2], Ayako MATSUOKA[*3],
Mariko TERAMOTO[*2], Shun IMAJO[*2]

ABSTRACT

The evaluation of the spacecraft-origin magnetic field noise ($B_{\_DCnoise}$) at the position of the sensor of Magnetic Field Experiments (MGF) onboard the Arase satellite has been performed. We examined the difference between the observation of the magnetic field with MGF and the Tsyganenko-Sitnov 04 (TS04) model field in DSI coordinates (ΔB_{DSI}) during the quiet time intervals. $\Delta B_{z, DSI}$ was ~0.7 nT on average, which indicates that the $B_{\_DCnoise}$ in the spin-axis direction is quite small. We conclude that the MGF data are well-calibrated and no large $B_{\_DCnoise}$ is included in the measured magnetic field. Although the difference between the MGF observations and the TS04 model in the X_{DSI} and Y_{DSI} directions was a few nT, it may be attributed to the TS04 model field, not an observational error of MGF.

1. Introduction

The Exploration of energization and Radiation in Geospace "Arase" (ERG) satellite was launched on 20 December 2016 to investigate the generation mechanism of the radiation belt and the dynamics of the geomagnetic storms in the Earth's inner magnetosphere (Miyoshi et al., 2018). It has an elliptical orbit with an inclination of ~31° with an apogee of ~6 R_E and a perigee altitude of ~460 km. Its spin period is ~8 s and the spin axis is approximately pointing to the Sun.

The Magnetic Field Experiment (MGF) instrument (Matsuoka et al., 2018) onboard Arase measures the three vectors of magnetic field by a triaxial fluxgate magnetometer with a sampling rate of 256 vectors/s. MGF has two dynamic ranges, ±60,000 nT and ±8,000 nT, which are switched depending on the background magnetic field, and are used for measurement at L < ~2 and L > ~2, respectively. Since the magnetic field controls the motion of the charged particles in space, quite accurate measurements of the background magnetic field is expected for MGF.

In general, magnetic field instruments include measurement errors caused by many factors, such as the sensor offset, the sensor sensitivity, the estimation of the sensor alignment, and the effects from the satellite body. To evaluate the sensor offset and the sensitivity, many experiments had been done before the satellite launch at the Japan Aerospace Exploration Agency (JAXA) Tsukuba Space Center (Teramoto et al., 2017). In addition, the errors of the sensor alignment are accurately calibrated when the data processing is performed. Although the MGF sensor is attached on the tip of the extendable MAST ~5 meters away from the satellite body to avoid the spacecraft-origin magnetic field noise ($B_{\_DCnoise}$), there may be non-zero $B_{\_DCnoise}$. Therefore, we estimate the $B_{\_DCnoise}$ in this report on the assumption that the ground calibration and the data processing calibration have been precisely performed, and we do not consider the sensor offset variations with the

temperature in this report.

The X-axis and Y-axis in Spinning Satellite Geometry Axis (SGA) coordinates rotate synchronized with the satellite spin, which enables us to estimate the $B_{DCnoise}$ in the X_{SGA} and Y_{SGA} components from the observational data. The $B_{DCnoise}$ can be removed by fitting a sinusoidal wave. However, we cannot estimate the $B_{DCnoise}$ in the Z_{SGA} component (i.e., spin-axis direction) from the observational data. To evaluate it, we compare the observational data to the Tsyganenko-Sitnov 04 (TS04) magnetic field model (Tsyganenko and Sitnov, 2005), which intends to express the strongly disturbed geomagnetic field on storm time and is often used to model the magnetic field in the inner magnetosphere. However, it should be noted that the difference between them may be generated by two factors, errors in the TS04 model and MGF. They will be discussed in Section 4.

2. Methods

We use the 8-s averaged magnetic field data on the geomagnetically quiet time during 23 March 2017 to 30 April 2018, excluding the period from 1 August to 3 November because of the malfunction of the dynamic range switching. In this time period, Arase covered almost all MLT ranges. The quiet time is determined by the 3-hour Kp index to be 0 or 0+. In addition, we impose the condition that the magnetic field does not significantly vary during one spin. This condition is implemented by a criterion that the dynamic range of the instrument is ±8,000 nT and the variation of the two successive spin-averaged magnetic field (δB) divided by the background magnetic field (Bt) is smaller than 0.006 ($\delta B/Bt < 0.006$). We compare the magnetic field data obtained by MGF to the TS04 model field in the selected time intervals in Despun Sun sector Inertia (DSI) coordinates, in which satellite spin is canceled and the Z-axis is almost along the spin axis. The discrepancy between the Z_{SGA} and Z_{DSI} coordinates is smaller than 1°. Input parameters for the TS04 model are solar wind dynamic pressure, Dst index, and IMF-Y, -Z values. In the present study, we use the SYM-H index instead of the Dst index, and interpolate their 1-min data to 8-s sampling of MGF.

3. Results

3.1. $\Delta B_{z,DSI}$

Figure 1a shows the histogram of the difference value between the magnetic field observed by MGF and TS04 model in the Z_{DSI} component (i.e., $\Delta B_{z, DSI}$) with a bin size of 0.1 nT. The mean value of $\Delta B_{z, DSI}$ is 0.66 ± 0.007 nT and the median value is 0.78 nT, which mean that the observational value is slightly larger than the TS04 model, but is quite closer to 0 nT. Figure 1b illustrates the distribution of the $\Delta B_{z, DSI}$ projected onto the R-MLT plane in Solar Magnetic (SM) coordinates with each mesh of 0.5 hr MLT by 0.5 R_E. White meshes show regions where no data satisfy the selection criteria. $\Delta B_{z, DSI}$ is generally be larger than 0 nT on the dayside, while it tends to be smaller than 0 nT on the nightside.
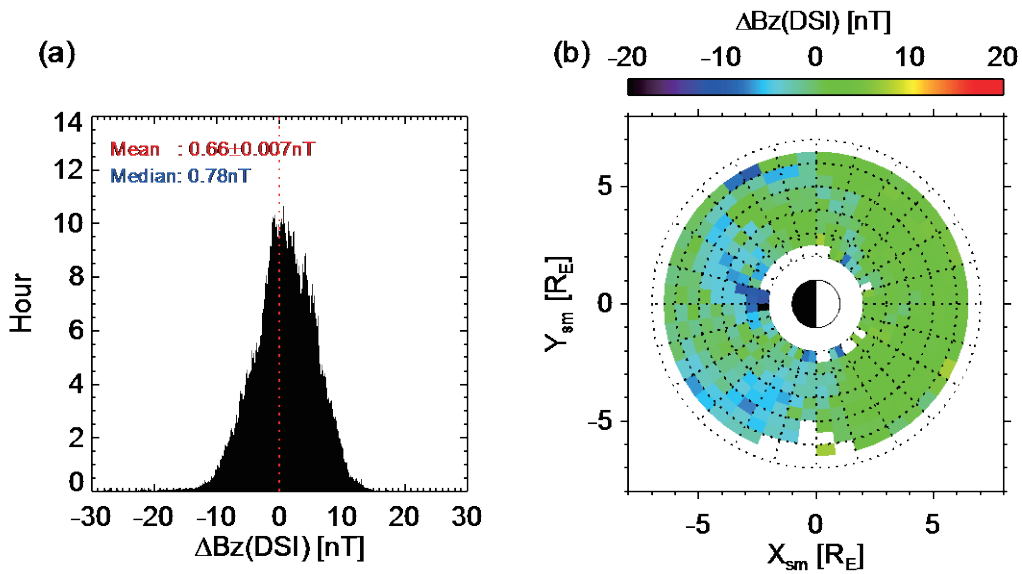
Fig. 1 (a) Histogram of the $\Delta B_{z,\,DSI}$ with a 0.1 nT bin. (b) Distribution of the $\Delta B_{z,\,DSI}$ projected onto the R-MLT plane in SM coordinates. Each mesh size is 0.5 hr MLT by 0.5 R_E.

3.2. $\Delta B_{x,\,DSI}$ and $\Delta B_{y,\,DSI}$

Figure 2 shows the histogram and distribution of $\Delta B_{x,\,DSI}$ in the same format as Figure 1. The mean value of $\Delta B_{x,\,DSI}$ is 2.36 ± 0.012 nT and the median value is 2.22 nT. $\Delta B_{x,\,DSI}$ is larger than $\Delta B_{z,\,DSI}$. The day-night asymmetry is not seen in Figure 2b.

Figure 3 gives the histogram and distribution of $\Delta B_{y,\,DSI}$. The mean value of $\Delta B_{y,\,DSI}$ is 4.81 ± 0.011 nT and the median value is 5.21 nT, which are much larger than those of $\Delta B_{z,\,DSI}$ and $\Delta B_{x,\,DSI}$. Also, the variance of the $\Delta B_{y,\,DSI}$ histogram is larger than those of $\Delta B_{z,\,DSI}$ and $\Delta B_{x,\,DSI}$. Figure 3b shows that $\Delta B_{y,\,DSI}$ is larger on the dayside than that on the nightside, and values are larger than 0 nT on both dayside and nightside. We find a specific orbit at dusk to midnight, where $\Delta B_{y,\,DSI}$ is quite smaller than the surrounding area.
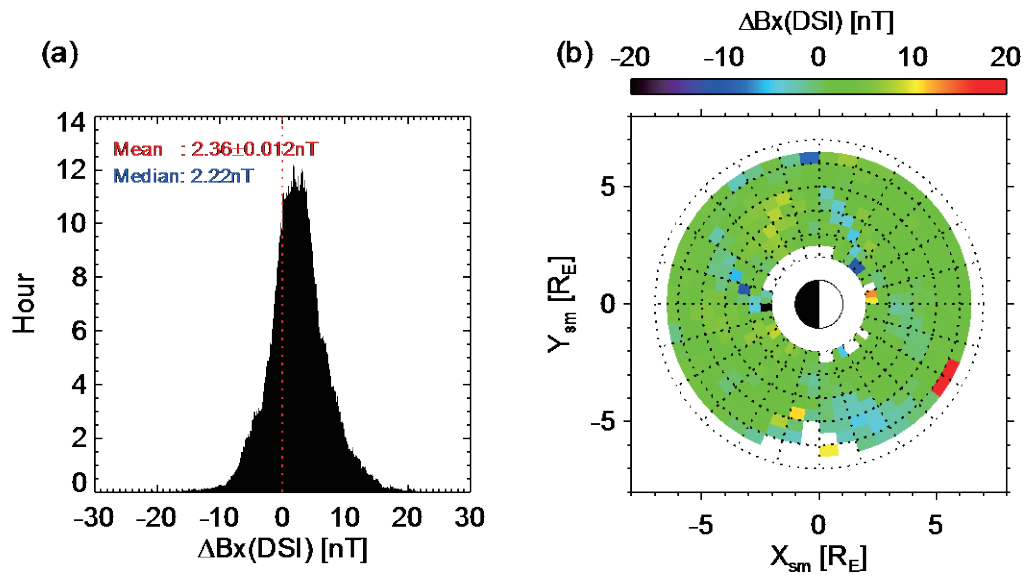
(a)

(b) ΔBx(DSI) [nT]

Fig. 2 Same as Figure 1 except for the $\Delta B_{x,\text{DSI}}$ component.

(a)
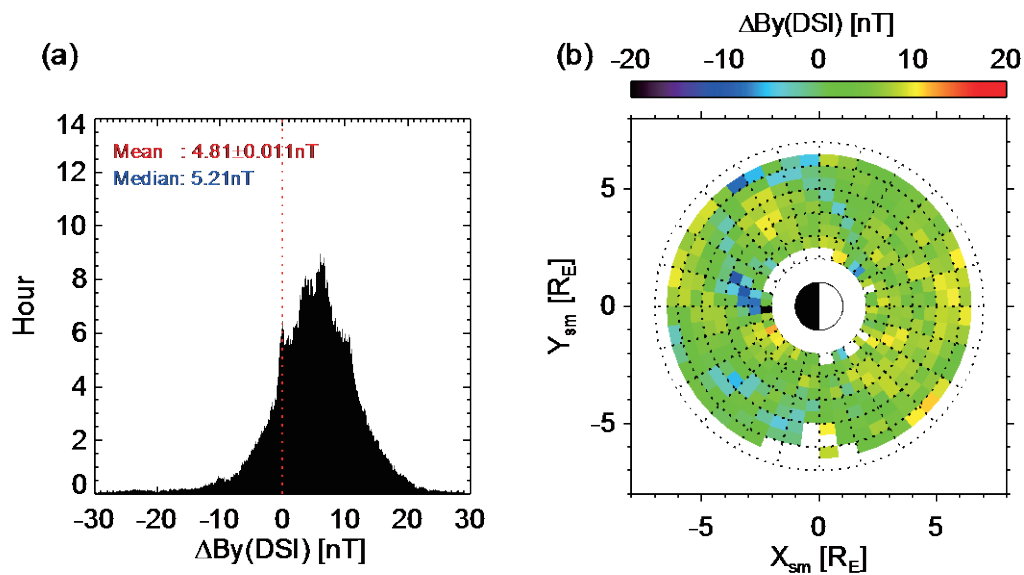

(b) ΔBy(DSI) [nT]

Fig. 3 Same as Figure 1 except for the $\Delta B_{y,\text{DSI}}$ component.

4. Discussion

4.1. $\Delta B_{z,\text{DSI}}$

The goal of this work is to estimate the $B_{\_DCnoise}$ in the Z_{DSI} direction (i.e., spin-axis direction). In the previous section, we obtained the histogram of $\Delta B_{z,\text{DSI}}$ in Figure 1a, and the result shows the $\Delta B_{z,\text{DSI}}$ to be quite small on average (0.66 nT). We conclude that the $B_{\_DCnoise}$ in the spin-axis direction is very small, and

the magnetic field data obtained by MGF are well-calibrated and contribute to the accurate measurements by Arase.

4.2. $\Delta B_{x, DSI}$ and $\Delta B_{y, DSI}$

The $\Delta B_{x, DSI}$ and $\Delta B_{y, DSI}$ were supposed to be small because the $B_{\_DCnoise}$ in the X_{DSI} and Y_{DSI} components can be removed by subtracting the sine-fitted data, if the TS04 model expresses the actual magnetic field correctly. However, the results showed large $\Delta B_{x, DSI}$ and $\Delta B_{y, DSI}$ (2.4 and 4.8 nT, respectively) as shown in Figures 2a and 3a. Although Z_{DSI} nearly directs to the Sun, the direction of X_{DSI} and Y_{DSI} axes varies according to the satellite positions. Yamamoto et al. (2019) investigated the direction of the X_{DSI} and Y_{DSI} axes, and found that these axes point roughly to –Y direction and +Z direction in SM coordinates, respectively. This indicates that the difference between the observational value and the TS04 model is the largest in the direction of the main field.

The possible causes of this large difference between the observational data and the TS04 model are considered to be due to an error in the measurement or the model. In this case, the $\Delta B_{x, DSI}$ and $\Delta B_{y, DSI}$ were large in spite of the expectation that they are small, and the difference in the component along the background geomagnetic field is larger than that in other components. Also, the day-night asymmetry of $\Delta B_{y, DSI}$ in Figure 3b may be due to the difficulty of the TS04 model to express accurately the compressed magnetic field and the elongated tail field. Thus, we suggest that the error is originated from the TS04 model.

We suppose two possible reasons for this error. The first one is that the TS04 model itself may overestimate the global current systems in the magnetosphere from the beginning, which influence on the magnetic field along the main field. The second reason may be the gradual decrease of the geomagnetic field of the Earth (i.e., magnetic moment). The TS04 model was created more than ten years ago. In recent year, the geomagnetic field becomes smaller. Although the model parameterization might have been correct when the model was created, the estimation of the external magnetic fields such as the magnetospheric current systems may not be appropriate for the present circumstances.

5. Conclusions

Our purpose of this report is to evaluate the spacecraft-origin magnetic field noise ($B_{\_DCnoise}$) at the sensor location onboard Arase. We compared the observational magnetic field of MGF to TS04 model field in the DSI coordinates during the quiet time intervals. $\Delta B_{z, DSI}$ was ~0.7 nT on average, which indicates that the $B_{\_DCnoise}$ in the spin-axis direction is quite small. We conclude that the MGF data are well-calibrated and provide accurate measurements of magnetic field. We also surveyed $\Delta B_{x, DSI}$ and $\Delta B_{y, DSI}$, and found that the difference is the largest in the direction of the ambient field. We attribute it to the TS04 model field, not an observational error of MGF.

REFERENCES

Matsuoka, A., M. Teramoto, R. Nomura, M. Nosé, A. Fujimoto, Y. Tanaka, M. Shinohara, T. Nagatsuma, K. Shiokawa, Y. Obana, Y. Miyoshi, M. Mita, T. Takashima and I. Shinohara (2018), The ARASE (ERG) magnetic field investigation, Earth, Planets and Space, 70:43, doi:10.1186/s40623-018-0800-1.

Teramoto M, Matsuoka A, Nomura R (2017), Ground calibration experiments of Magnetic field experiment on the ERG satellite (Japanese), JAXA Research and Development Memorandum JAXA-RM-16-003.

Tsyganenko, N. A., and M. I. Sitnov (2005), Modeling the dynamics of the inner magnetosphere during strong geomagnetic storms, J. Geophys. Res., 110, A03208, doi:10.1029/2004JA010798.

Miyoshi, Y., I. Shinohara, T. Takashima, K. Asamura, N. Higashio, T. Mitani, S. Kasahara, S. Yokota, Y. Kazama, S-Y. Wang, S.W. Tam, P. Ho, Y. Kasahara, Y. Kasaba, S. Yagitani, A. Matasuoka, H. Kojima, Y. Katoh, K. Shiokawa, K. Seki (2018), Geospace Exploration Project ERG, Earth, Planets and Space, doi: 10.1186/s40623-018-0862-0.

Yamamoto, K., S. Oimatsu, M. Nosé, A. Matsuoka, M. Teramoto, S. Imajo (2019), DC component of spacecraft-origin magnetic field noise at the Arase/MGF sensor: (1) Evaluation with Tsyganenko 89 model, JAXA Research and Development Report, JAXA-RR-18-005E, 10.20637/JAXA-RR-18-005E/0004.

JAXA Research and Development Report JAXA-RR-18-005E

Calibration and Evaluation of Data from the Magnetometer (MGF) Onboard the Arase (ERG) Spacecraft